Report Prepared by:

David Dukeman
Hani Freij
Alberto A. Sagüés
Christopher Alexander

FINAL REPORT

FIELD DEMONSTRATION OF TENDON IMAGING METHODS

Contract No. BDV25-977-52

Final Report to Florida Department of Transportation

Continuing PI: Christopher Alexander, University of South Florida, Tampa, FL.
Initiating PI: Alberto Sagüés.

Department of Civil and Environmental Engineering

COLLEGE OF ENGINEERING

Tampa, FL 33620
July, 2019

DISCLAIMER

The opinions, findings, and conclusions expressed in this publication are those of the author(s) and not necessarily those of the Florida Department of Transportation or the U.S. Department of Transportation.

UNIVERSAL CONVERSION TABLE

SI* (MODERN METRIC) CONVERSION FACTORS

APPROXIMATE CONVERSIONS TO SI UNITS

SYMBOL	WHEN YOU KNOW	MULTIPLY BY	TO FIND	SYMBOL
		LENGTH		
in	inches	25.4	millimeters	mm
ft	feet	0.305	meters	m
yd	yards	0.914	meters	m
mi	miles	1.61	kilometers	km
		AREA		
in^2	square inches	645.2	square millimeters	mm^2
ft^2	square feet	0.093	square meters	m^2
yd^2	square yard	0.836	square meters	m^2
ac	acres	0.405	hectares	ha
mi^2	square miles	2.59	square kilometers	km^2
		VOLUME		
fl oz	fluid ounces	29.57	milliliters	mL
gal	gallons	3.785	liters	L
ft^3	cubic feet	0.028	cubic meters	m^3
yd^3	cubic yards	0.765	cubic meters	m^3
		NOTE: volumes greater than 1000 L shall be shown in m^3		
		MASS		
oz	ounces	28.35	grams	g
lb	pounds	0.454	kilograms	kg
T	short tons (2000 lb)	0.907	megagrams (or "metric ton")	Mg (or "t")
		TEMPERATURE (exact degrees)		
^0F	Fahrenheit	5 (F-32)/9 or (F-32)/1.8	Celsius	^0C
		ILLUMINATION		
fc	foot-candles	10.76	lux	lx
fl	foot-Lamberts	3.426	$candela/m^2$	cd/m^2
		FORCE and PRESSURE or STRESS		
lbf	poundforce	4.45	newtons	N
lbf/in^2	poundforce per square inch	6.89	kilopascals	kPa

APPROXIMATE CONVERSIONS FROM SI UNITS

SYMBOL	WHEN YOU KNOW	MULTIPLY BY	TO FIND	SYMBOL
		LENGTH		
mm	millimeters	0.039	inches	in
m	meters	3.28	feet	ft
m	meters	1.09	yards	yd
km	kilometers	0.621	miles	mi
		AREA		
mm^2	square millimeters	0.0016	square inches	in^2
m^2	square meters	10.764	square feet	ft^2
m^2	square meters	1.195	square yards	yd^2
ha	hectares	2.47	acres	ac
km^2	square kilometers	0.386	square miles	mi^2
		VOLUME		
mL	milliliters	0.034	fluid ounces	fl oz
L	liters	0.264	gallons	gal
m^3	cubic meters	35.314	cubic feet	ft^3
m^3	cubic meters	1.307	cubic yards	yd^3
		MASS		
g	grams	0.035	ounces	oz
kg	kilograms	2.202	pounds	lb
Mg (or "t")	megagrams (or "metric ton")	1.103	short tons (2000 lb)	T
		TEMPERATURE (exact degrees)		
^0C	Celsius	1.8C+32	Fahrenheit	^0F
		ILLUMINATION		
lx	lux	0.0929	foot-candles	fc
cd/m^2	$candela/m^2$	0.2919	foot-Lamberts	fl
		FORCE and PRESSURE or STRESS		
N	newtons	0.225	poundforce	lbf
kPa	kilopascals	0.145	poundforce per square inch	lbf/in^2

*SI is the symbol for the International System of Units. Appropriate rounding should be made to comply with Section 4 of ASTM E380.

TECHNICAL REPORT DOCUMENTATION PAGE

1. Report No.	2. Government Accession No.	3. Recipient's Catalog No.
4. Title and Subtitle FIELD DEMONSTRATION OF TENDON IMAGING METHODS		5. Report Date July, 2019
		6. Performing Organization Code
7. Author(s) D. Dukeman, H. Freij, A. Sagüés and C. Alexander		8. Performing Organization Report No.
9. Performing Organization Name and Address Department of Civil and Environmental Engineering University of South Florida (USF) Tampa, FL 33620		10. Work Unit No. (TRAIS)
		11. Contract or Grant No. BDV25-977-52
12. Sponsoring Agency Name and Address Florida Department of Transportation 605 Suwannee St. MS 30 Tallahassee, Florida 32399 (850)414-4615		13. Type of Report and Period Covered Final Report 01/12/2018-07/31/2019
		14. Sponsoring Agency Code
15. Supplementary Notes		

16. Abstract: Inadequate grouting is associated with corrosion of post-tensioning steel in grouted tendons used in construction applications. A nondestructive method capable of revealing grout deficiencies of external tendons was developed under concurrent FDOT Project BDV25-977-24. The method uses impedance and magnetic measurements to produce an image of the cross-section of the tendon, flagging air voids and other deficiencies in the grout portion that is between the outer strand bundle envelope and the inner surface of the tendon polymer duct. In this project an operating prototype of a unit using the method was designed and constructed, field demonstrated in FDOT bridges, and delivered for use by FDOT. The unit is capable of operation in commonly used 4.5-inch diameter tendons, tolerant of elliptical tendon perimeters, and designed for fast and economic replication. Operation does not require highly specialized personnel. This report describes unit design, field and laboratory experience, and operating instructions of a unit constructed and delivered as part of the project.

17. Key Word Grout; Highway bridges; Prototypes; Sensors; Tendons (Materials)	18. Distribution Statement No Restriction This report is available to the public through the NTIS, Springfield, VA 22161

19. Security Classif. (of this report) Unclassified	20. Security Classif. (of this page) Unclassified	21. No. of Pages: 48	22. Price

ACKNOWLEDGEMENTS / NOTICE

The authors acknowledge the assistance of Dr. Michael Celestin for valuable advice on data acquisition instrumentation and software, and Jordan-Riber Smith for assistance in software code. The support of the Corrosion group of the FDOT State Materials Office in conducting the field evaluations is much appreciated. This report contains information related to Patent US 9,651,357 Bl as well as other internal disclosures subject to applicable intellectual property rights and patent(s) pending by the University of South Florida.

EXECUTIVE SUMMARY

Inadequate grouting has been found to be associated with corrosion of post-tensioning steel in grouted tendons used in construction applications. Local grouting deficiencies include voids where bleed water existed and was later reabsorbed elsewhere or evaporated, regions of chalky low strength grout, and regions where excessive water content or even free water is present [1,2]. In those zones, mechanical bonding of strand to the grout is degraded, and of more concern, the strand steel risks corrosion failure. As tendons are critical structural components, it is important to detect those deficiencies during inspections of existing bridges and, if possible, during the construction phase of new bridges so that early remedial measures can be taken.

In response to that need, FDOT sponsored Project BDV25-977-24 “Development of Tendon Imaging Sensor”. The objective of that project was to develop for field application a non-intrusive method to image strand position and grouting anomalies inside the cross-section of external post-tensioned tendons. Furthermore, the project developed a laboratory prototype of that technology. The objectives of this project were to develop and produce a strand location and grout deficiency imaging sensor prototype, suitable for field operation on external post-tensioned tendons and to demonstrate operation in FDOT bridges.

An operating Field Tendon Imaging Unit (FTIU) was designed, constructed, and delivered to FDOT. The FTIU uses impedance and magnetic measurements to produce an image of the cross-section of an external post-tensioned tendon in a portable computer, flagging air voids and other deficiencies in the grout portion that is between the outer strand bundle envelope and the inner surface of the tendon polymer duct. The cross-section image includes the envelope of the strand bundle inside the tendon (from the magnetic measurements) and a color-coded indication of the condition of the grout in the space between the strand bundle and the inner surface of the tendon duct (from the impedance measurements). The FTIU contains a magnet with force sensor and a flexible capacitive plate that follows the tendon duct perimeter during rotation around the tendon. The system accommodates external tendons with a 4.5-inch outer diameter and has a flexible design to fit other common duct sizes in FDOT bridges. The FTIU is short and uses a clamshell arrangement to fit around the tendon with small (e.g., <1.5-inch) overburden, thus allowing for imaging in tight spaces without interfering with other tendons or structural members. The FTIU has a robust construction that is suitable for extended field use.

It takes only about 10-seconds to acquire a cross-section image, which is obtained by manually rotating the FTIU around the tendon and is displayed immediately by a laptop computer. The computer powers the FTIU by normal low-demand battery function, so the system is fully portable.

Operation does not require specialized operator training, and equipment can be reproduced at low cost and loaded with executable software produced by the project, thus providing an economic and rapid tendon assessment method capable of simultaneous deployment of multiple units. The FTIU provided consistent and descriptive images of the strand bundle envelope within the tendon. With appropriate calibration, the FTIU also reliably imaged full voids of lateral dimensions comparable to the size of the capacitive plate and larger. Those voids are flagged by color-coding the zone between the strand bundle envelope and the inner surface of the duct. Sensitivity to smaller or internal void is limited; when detected, a partial color display scheme is shown. Refined detection can be made by calibration with a tendon that has known conditions.

Detection of high water content grout is mainly an experimental feature given that such content causes only a fractional reduction in the impedance at the frequency used in the FTIU.

Two field visits were made to the Ringling Bridge, demonstrating application on four test places with multiple variations of system wiring and grounding, as well as to establish repeatability. The field results demonstrated stability of response under grounding and wiring variations, as well as repeatability within a given condition. All images were successfully and rapidly acquired, consistently identifying the main pattern of strand locations for a given test place. The FTIU retained physical integrity through extensive repeat field testing and no breakdown or need for repair took place. Tests conducted on the tendons at different places with respect to deviation blocks revealed strand clustering consistent with the orientation of the deviation block and with the extent of the deviation.

All the field images obtained at the Ringling Bridge were consistent with sound grout, with no void or other detectable deficiency at any of the places examined, likely reflecting prior extensive repairs there. Consequently illustrations of the ability to identify selected types of deficiencies on a laboratory tendon mockup were presented instead.

TABLE OF CONTENTS

LIST OF FIGURES

LIST OF TABLES

1. BACKGROUND AND OBJECTIVES

Inadequate grouting has been found to be associated with corrosion of post-tensioning steel in grouted tendons used in construction applications. Local grouting deficiencies include voids where bleed water existed and was later reabsorbed elsewhere or evaporated, regions of chalky low strength grout, and regions where excessive water content or even free water is present [1,2]. In those zones, mechanical bonding of strand to the grout is degraded, and more of concern, the strand steel risks corrosion failure. As tendons are critical structural components, it is important to detect those deficiencies during inspections of existing bridges and, if possible, during the construction phase of new bridges so that early remedial measures can be taken.

In response to that need, FDOT sponsored Project BDV25-977-24 “Development of Tendon Imaging Sensor” [3]. The objective of that project was to develop for field application a non-intrusive method to image strand position and grouting anomalies inside the cross-section of external post-tensioned tendons. Furthermore, the project was to develop a laboratory prototype of that technology. The project, being conducted at the University of South Florida, succeeded in creating the basic units of a strand imaging sensor and a complementary grout deficiency sensor. The sensing system is both non-intrusive and capable of rapid operation and low-cost development. The sensors are integrated into a single unit. Project BDV25-977-24 concluded with development of a laboratory demonstration unit, but did not include construction of a unit suitable for use and demonstration at external tendons in a bridge in the field. That development and deployment as a continuation of effort is the subject of the present work.

Per the above discussion, the objectives of this project were to:

1. Based on results from BDV25-977-24, develop and produce a strand location and grout deficiency imaging sensor prototype, suitable for field operation on external post-tensioned tendons.

2. Demonstrate operation of the imaging sensor in one or more FDOT bridges, and provide the working prototype to FDOT.

2. APPROACH AND TASKS

The project proceeded along the following tasks.

2.1 Task 1: Adapt laboratory unit for field operation.

Progress under BDV25-977-24 resulted in development and demonstration of a laboratory unit that produced, by external nondestructive sensing, an image of the cross-section of an external tendon. The image revealed the position of the envelope of the steel strand bundle inside the cross-section, and revealed also irregularities, if present, of the normally grout-filled space between the strand envelope and the inner surface of the polymer duct of the external tendon.

The principle of operation involved two stages conducted concurrently by the operating unit. The first stage involved determining the position of the strand bundle envelope by means of a magnetic sensing system, using one or more magnets that rotated around the tendon [3]. The force acting on the magnets was measured by an electronic transducer and converted via time-delay deconvolution and force-distance function modeling into radial positon of the strand envelope within the tendon. Figure 1 illustrates the basics of the arrangement and a resulting externally obtained bundle envelope image. Comparison with the actual strand configuration in the tendon indicated close agreement. Imaging was rapid (typically < 10-seconds) and reproducible.

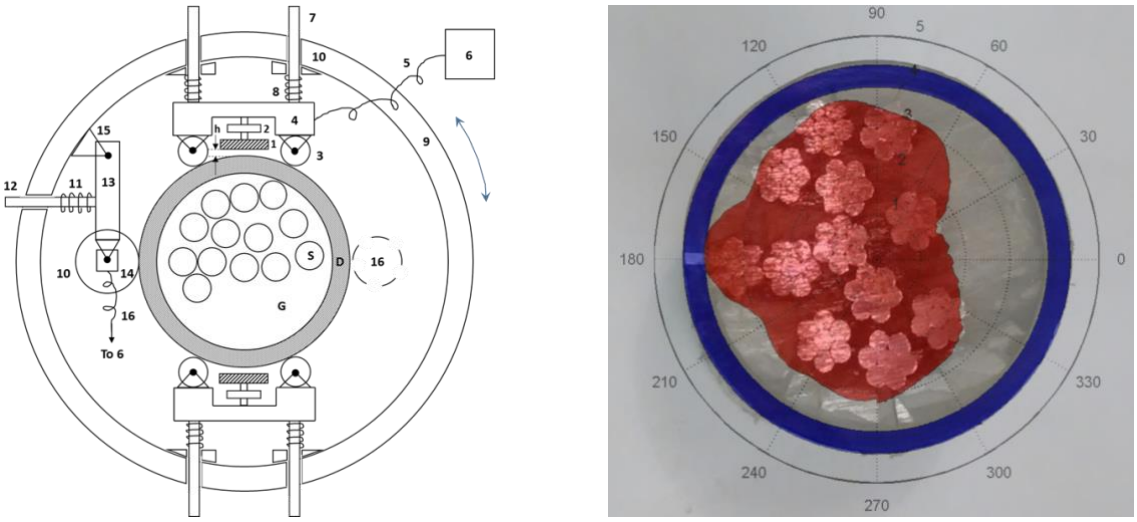

Figure 1 Left: Magnetic strand position imaging method developed under BDV25-977-24 [3]. Right: Example of strand envelope recovery on a cross-section of a tendon segment. Duct outer diameter is ~3.5-inch; duct wall section represented by the blue ring. The recovered envelope (red) has been superimposed on an actual picture of the tendon segment cross-section at the end of the segment. Covered under Patent US 9,651,357 B1 [4] and any other applicable USF intellectual property rights.

The second stage, illustrated in Figure 2 (Left), involved measuring the high frequency electric impedance between an externally traveling metallic plate of finite size in contact with the outer surface of the polymer duct, and the strand bundle (which by the nature of the anchoring system has full mutual electric contact between all the strands). The impedance may be seen as the sum of the duct wall impedance -nearly constant- and the impedance of the grout space intervening between the duct and the strand bundle. In the case of normal grout the grout space impedance is expected to be a finite, modest value given by the appreciable effective dielectric constant and conductance of sound grout. Deficiencies such as grout voids would on the other hand diminish the conductive path and average dielectric constant, thus resulting in a marked increase in impedance compared to that of sound grout. For imaging, first the value of the impedance as function of angular position of the plate is determined by rotating the plate around the tendon perimeter. The constant contribution of the duct wall is then subtracted so as to focus on the impedance of the grout space. More than one plate may be used as well to reduce need for rotating one full revolution.

The second stage impedance result is then numerically evaluated and graphically displayed, together with the first stage strand envelope pattern, to flag the presence of grout irregularities in the space between the strand envelope and the inner surface of the tendon duct. An illustration of the composite image thus obtained is shown in Figure 2 (Right).

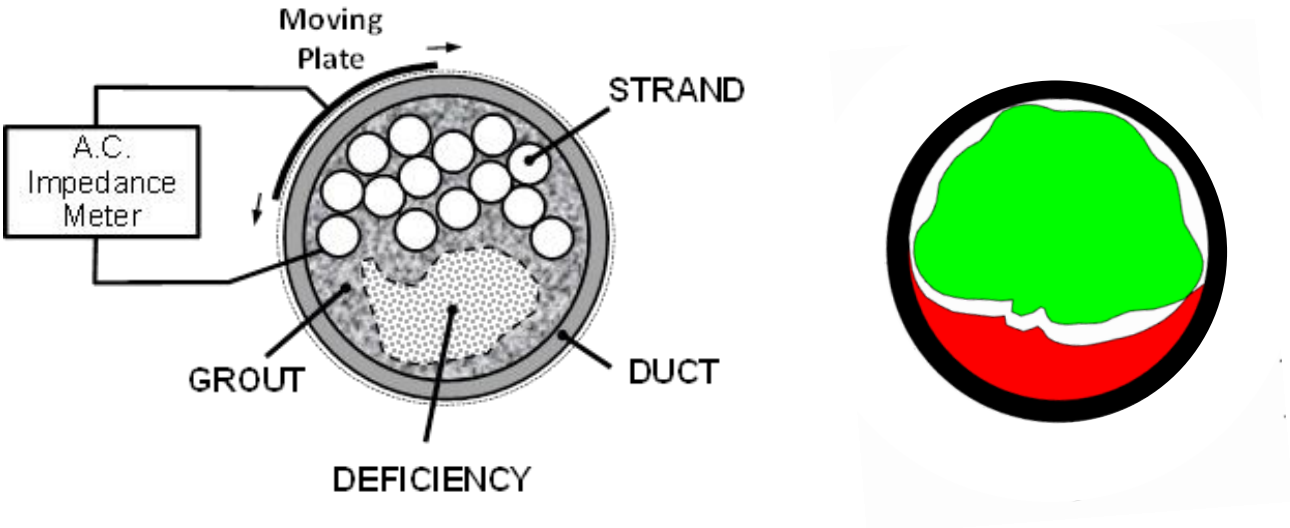

Figure 2 Left: Deficiency detection method via impedance measurements developed under BDV25-977-24. The data are processed taking into account the information on strand position previously obtained with the magnetic imaging system. Right: Adapted illustration of the result of integrating both imaging stages shoeing the strand bundle (green), some zones of normal grout (white) and a void region (red). Covered under Patent US 9,651,357 B1 [4] and any other applicable USF patent applications.

In the simplest arrangement both a magnetic and an impedance sensors can be accommodated at opposite points of the circumference of a rotating sensing assembly, creating an integrated imaging unit that can be positioned along successive places on the tendon length. Signal conditioning and initial processing take place on an onboard electronic processor placed at the unit. Further processing is handled by software at a computer linked to the traveling combined module. The resulting images can be examined in succession resulting in a tunneling view of the tendon interior with flagged grout irregularities. This concept was developed and implemented in a compact design for field testing in the present project, with details provided in the following sections. This unit is described in Chapter 3 of this report.

2.2 Task 2: Field tests, demonstrations, and optimization.

Field tests using the unit that was constructed under Task 1 were conducted in post-tensioned structures chosen in consultation with the Project Manager and appropriate FDOT offices. The tests were conducted in cooperation and coordination with personnel from the State Materials Office (SMO) concerning access to the site and initial familiarization of FDOT personnel with the methodology and equipment to be used.

The imaging unit and operating software was optimized and reevaluated via field tests. The improved system was implemented accordingly and a finalized working prototype was produced and delivered to FDOT with operating instructions, per description in Chapter 3 and manual attached as Appendix 1. The field test experience is summarized in Chapter 4 of this report.

3. FIELD TENDON IMAGING UNIT DESIGN AND OPERATION

3.1 Design and Construction

The Field Tendon Imaging Unit (FTIU) was adapted from the findings of project BDV25-977-24 by designing with the following target performance goals:

- Fit tendons of size comparable to those used in the Ringling Bridge (~4.5-inch diameter).
- Flexible design to accommodate other common tendon diameter values.
- Clamshell configuration for immediate mounting on and removal from tendon.
- Overburden on tendon radius <~1.5-inch. Unit length body < 5-inch.
- Accommodate tendons with cross-section deviating from circular into elliptical shape up to major/minor axis ratio (ellipticity) of 1.1.
- Acquisition and display an imaged cross-section within 10-seconds.
- Automatic data storage.
- Portable operation with a computer laptop.
- Minimal need for operator training and processing of data.
- Low cost of construction and operation.

The FTIU physical arrangement is shown schematically and in photographs in Figures 3 and 4. The clamshell assembly is a manually rotated unit that contains a single sensing magnet and a single capacitive plate, set approximately 180-degrees from each other and both covering the same cross-section of the tendon in one full turn.

The magnet has a magnetic moment in the order of ~4 $A \cdot m^2$ and creates attractive forces to the strand bundle that can reach ~1N at the closest operating distances. The magnet is attached to a rigid force sensing element of the type used in electronic balances, and rides in the center of an array of 4 ball bearing rollers, maintaining a minimal distance h in the order of 2 mm above the outer surface of the duct, as long as ellipticity does not exceed the design target.

The capacitive sensing plate is made of articulated stainless steel elastic segments, of the type used in wristwatch bands. The plate is 5 cm x 5 cm square, and is pressed closely against the surface of the duct by two springs. This construction is robust and durable and allows the plate to tightly fit during rotation against the duct eliminating intervening air space. Despite that, the construction minimizes friction that would otherwise displace the plate from its intended position, as well as it tolerates the minor duct surface scratches and similar irregularities normally present in tendons in the field. The construction also allows for correct operation even if the surface has ellipticity within the design target.

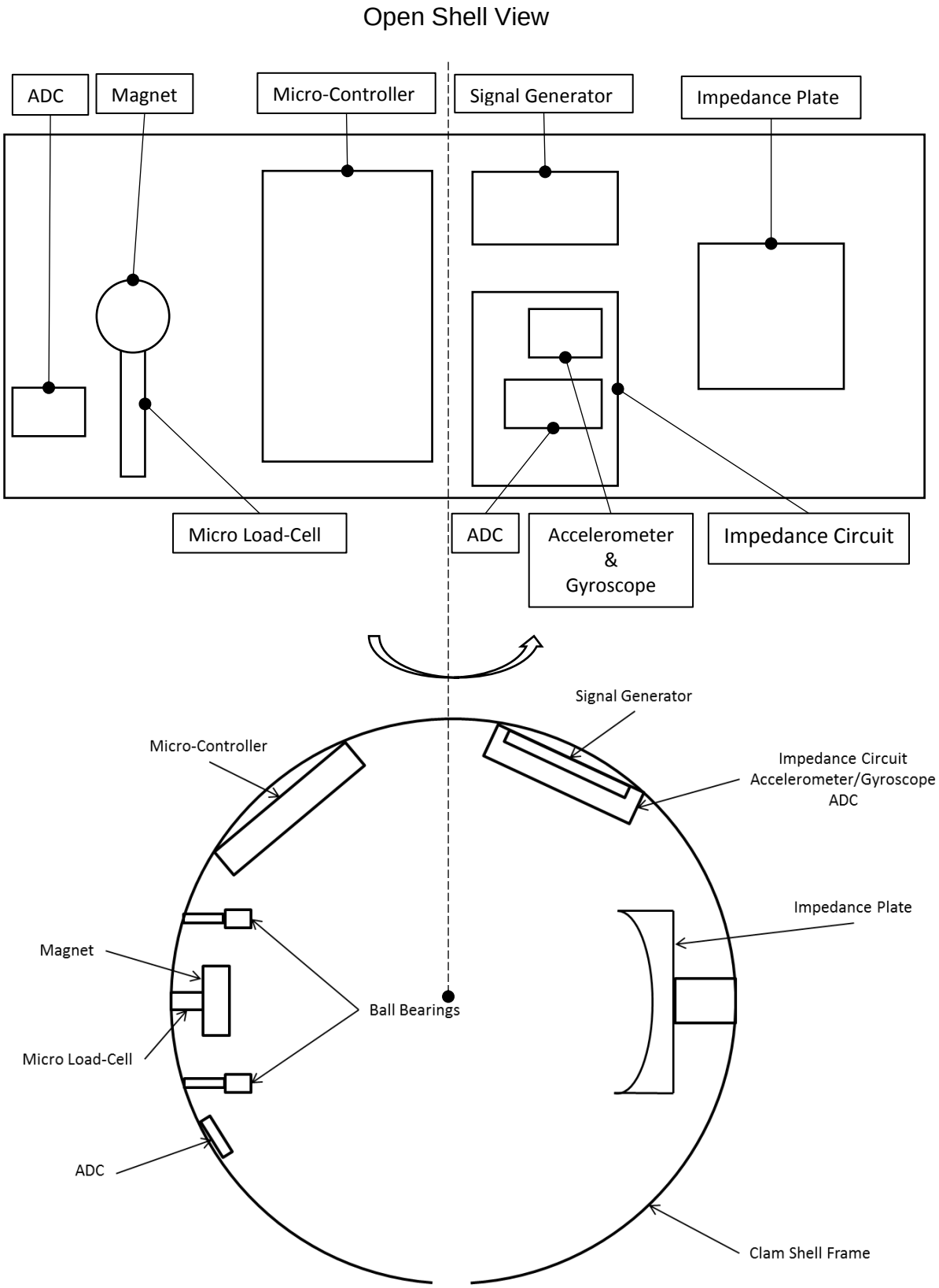

Figure 3 Schematic diagram of the FTIU physical arrangement. Patent Pending.

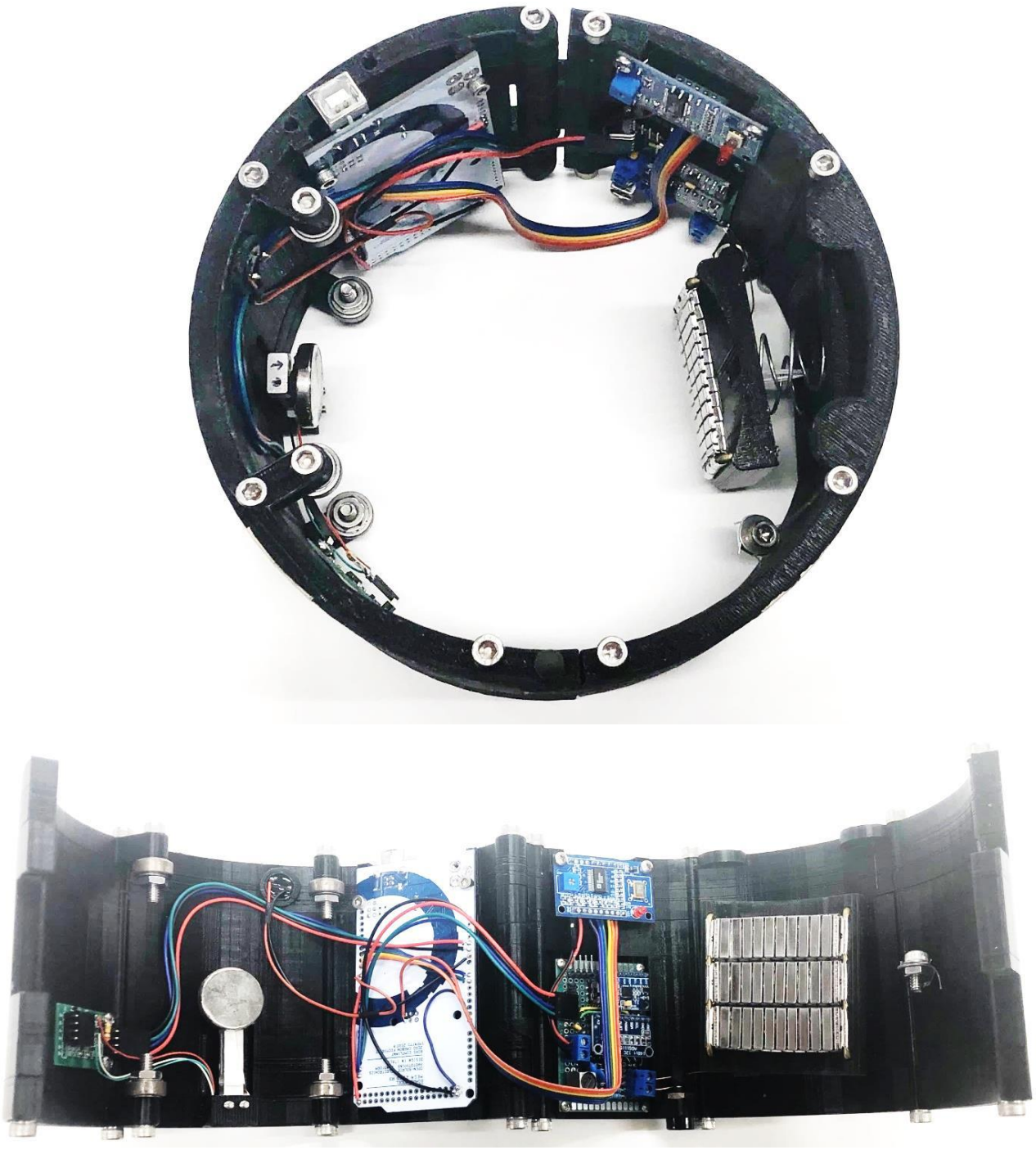

Figure 4 FTIU physical arrangement. Patent Pending.

For operation, detailed in Appendix 1, the unit is first calibrated and then the clamshell is closed on the tendon place to be imaged. The unit is then manually rotated one full turn, producing a beep signal when the turn is completed. During rotation the unit produces, angular rotation, magnetic force, and impedance data that are sent together with inclination data to the laptop computer via a USB cable. Immediately afterwards the data are processed, and an image of the cross-section is displayed on the computer screen. The instrumentation used for data generation and processing is schematically described in Figure 5

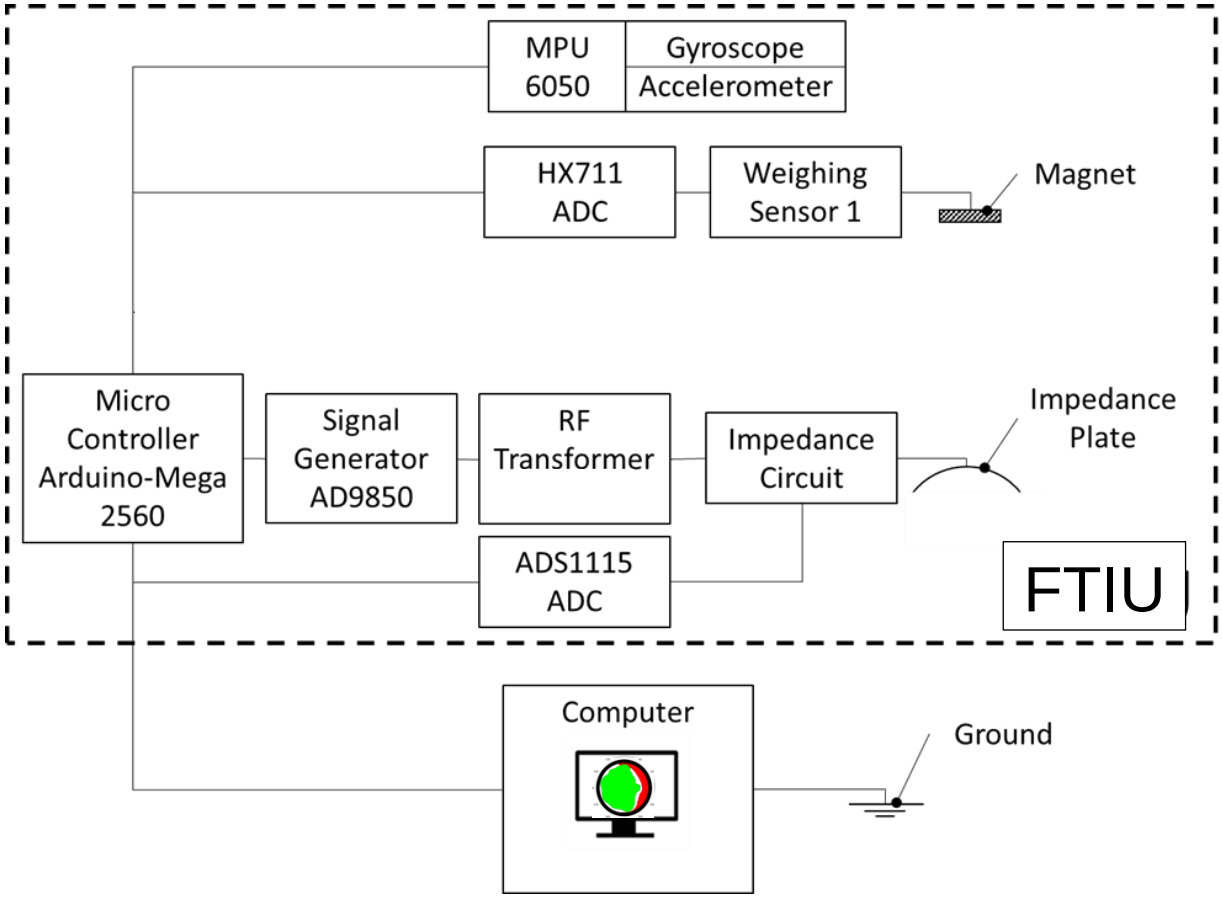

Figure 5 FTIU instrumentation block diagram. Patent Pending.

The FTIU with the laptop is a self contained system that can operate freely without a need for an electrical outlet. Within the FTIU, all the components are connected to a main microcontroller (Arduino Mega 2560 board) which does the following:

- Powers the signal generator which originates a 1-MHz signal for impedance measurements.
- Powers the magnetic sensor, and a gyroscope/accelerometer board.
- Transmits all the data from the components, the time, angular position, magnetic forces, impedance measurements, and gyroscope/accelerometer measurements to the laptop computer which then analyzes the data via executable MATLAB code.

Construction and functional features are:

- The FTIU was assembled on a 3D-printed clam-shell frame (Figure 4) printed from a polylactide (PLA) thermoplastic filament which also contains the onboard Arduino Mega2650 microcontroller and the various electronic circuit boards.
- The impedance module consists of a driving circuit that has a 1-MHz signal generator built with an AD9850-based board. The signal goes to a *dc* isolating radio frequency (RF) transformer that feeds an RF bridge provided with a diode rectifier. The rectified and filtered bridge output is proportional to the modulus of the impedance between the plate and the strand bundle. That signal is then read by an ADS1115-based analog-digital converter (ADC) board that communicates with the microcontroller.
- The magnetic strand position detection module consists of a HX711 ADC board wired to a micro load cell with the magnet attached to the free end of the load cell. The output goes to the microcontroller.
- Readings of the accelerometers and high-precision gyroscope, both contained in the MPU6050 circuit board, are used by the computer to determine tendon inclination and angular position of the FTIU. As a result, no physical contact with a riding wheel or similar transducer is needed for angular position tracking (which had been used in a previous version of the magnetic imaging method).
- The Arduino Mega2650 microcontroller is sent commands and returns data to the laptop computer per operator prompts.
- The outer perimeter of the entire FTIU is contained within ~1.5-inch from the external HDPE duct perimeter.

3.2 Operation and Data Management

The operating software is written for a Windows 10 platform in the form of an executable MATLAB code. Operation is detailed in the User Guide in Appendix 1. The following is a functional description of the way in which data are acquired and processed.

As the FTIU is rotated, it sends to the computer an array of applicable data with seven operating columns. The first column has time t at approximately 0.1-second intervals recorded in ms. The 2nd and 3rd columns contain the synchronous force, $F_R(t)$, sensed by the magnet force transducer and the impedance modulus, Z, reported by the impedance meter. Columns 4 to 6 contain accelerometer readings ax, ay, and az for the x (lengthwise tendon axis), y, and z axes, respectively. Column 7 contains gyroscope readings gx for the x axis. The overall array covers a time interval on the order of 10-seconds, or about 100 rows.

The FTIU microcontroller integrates internally a reading of gx to determine when the FTIU has completed a full rotation around the x axis and provides a beep sound to signal the operator that the rotation is completed. The ay and az readings are used to trigonometrically compute the value of the angle Θ_R with respect to the line joining the center of the tendon cross-section and the apex (Figure 6) at the moment the rotation has begun. That value is recorded, and then the reading gx is integrated to compute the increase of Θ_R as time progresses. The constant tendon slope angle Θ_S is trigonometrically calculated via the combined values of ax, ay, and az, and used together with Θ_R for gravitational force corrections as shown next. Information on the FTIU geometry is used to correctly register the data from the accelerometer/gyroscope, force sensor, and impedance sensor, by adding the appropriate angular offsets to compensate for their different angular positions on the FTIU perimeter. All relevant system parameters are introduced in the following and further listed in Table 1.

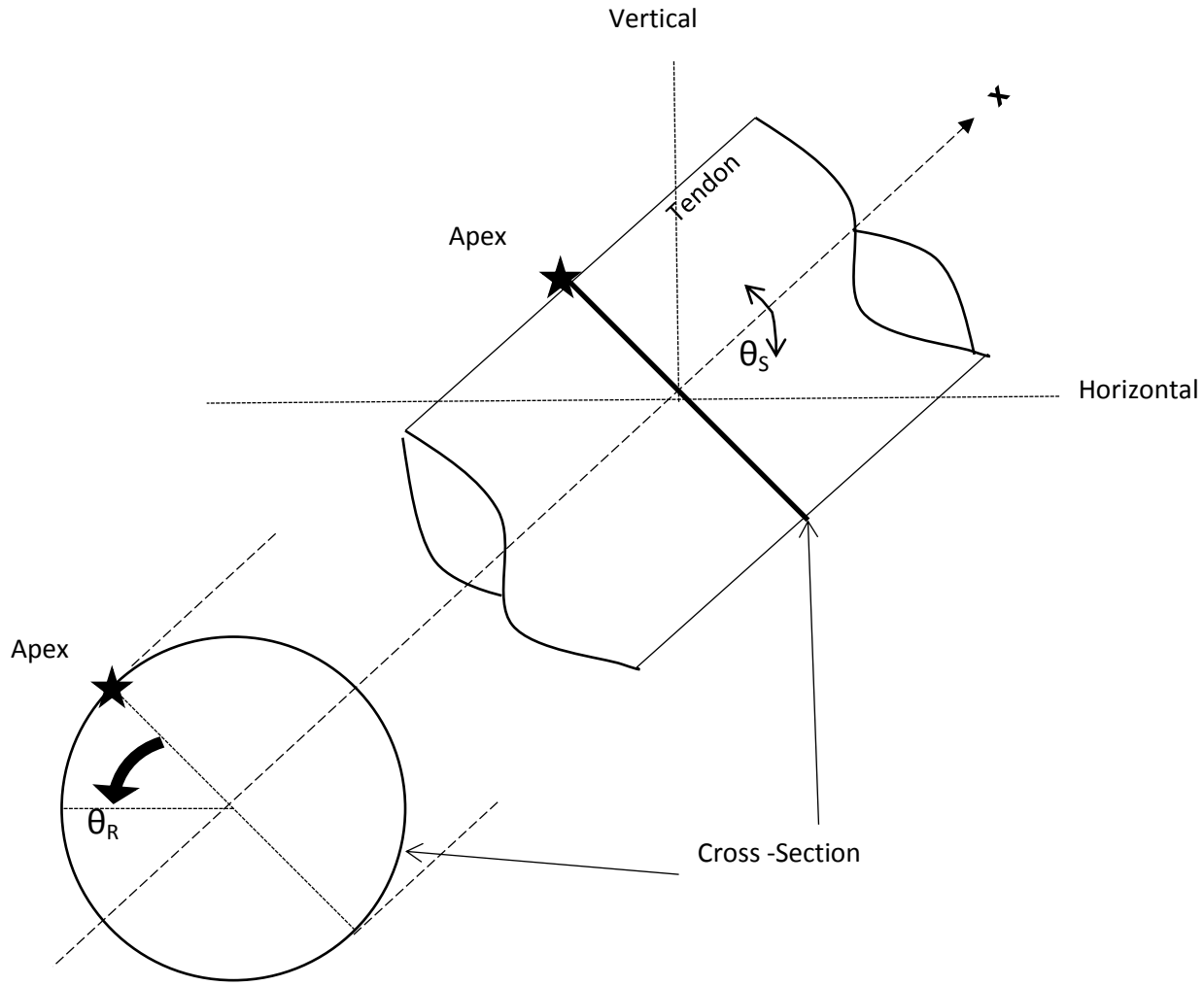

Figure 6 Side and gyrated section view of a sloping tendon, illustrating tendon slope angle Θ_S and FTIU rotation angle Θ_R (cross-section shown as viewed from the lower end). The accelerometer and gyroscope x axes are oriented along the tendon length.

The magnet force information is transferred to the computer in the form values F_R in sensor units and synchronous with the time array. The sensor has been pre-calibrated, one sensor unit corresponding to ~$3 \cdot 10^{-3}$ N, and auto-zeroed to remove any native signal offset so 0 units correspond to 0 N.

The recorded value of F_R is affected to some extent by convolution with the force-sensor and data processing step function response - an effect not unlike motion blur in a photograph with an unsteady camera. To sharpen the response, the $F_R(t)$ signal is subject to deconvolution based on independent determination of the step response of the sensor, simplified as an exponential response with a characteristic time τ. The default value for that parameter is τ=0.065 and the signal is processed accordingly as indicated in [3] to obtain a deconvoluted force function F(t).

If the tendon orientation is other than vertical, as the FTIU turns the weight of the magnet W_M will introduce a gravitational component of the force recorded by the sensor. That component must be subtracted from F to obtain the force F_M due to magnetic attraction only. Referring to Figure 6, for a tendon slope Θ_S and an angle of rotation Θ_R (measurement of those values described later) the gravitational component correction is then

$$F_M = F - W_M \cos\Theta_S \cos\Theta_R \qquad \text{(Eq. 1)}$$

As W_M is ~0.2 N, the gravitational component is significant enough for correction to be necessary. There is also a centripetal force component to F, but calculations indicated at the angular speeds and dimensions involved here the contribution is usually small enough to be neglected.

An additional correction to F_M is tentatively introduced for cases where the grout may have a distinct magnetic behavior, whereby the relative magnetic permeability μ_{grout} is significantly in excess of 1. As noted in [5], some grouts may have values approaching $\mu_{grout} = 1.02$, a situation also encountered in some cementitious materials [6]. Experimentation with the magnet placed at distances in the order of 1cm from hardened samples of those grouts indicated attractive forces in the order of $1 \cdot 10^{-2}$ N (~ 3 sensor units). Consequently, a subtractive correction constant equal to $(\mu_{grout} - 1) \cdot 10^2$ was applied tentatively to F_M based on the assumed value of the grout relative permeability. The correction defaults to zero for cases of assumed absence of grout magnetic behavior.

The value of F_M after all corrections is then converted into distance d_{MS} from center of magnet to strand bundle envelope position per the procedure indicated in [3] per:

$$d_{MS} = (k/F_M)^{1/n'} \qquad \text{(Eq. 2)}$$

With parameter values k = 621.5 (sensor units • $cm^{n'}$) and n' = 3.185 obtained by calibration with a known steel strand position with respect to the magnet.

The value of d_{MS} is then converted into distance d_C from the center of the tendon to the strand bundle envelope by

$$d_C = D/2 - (d_{MS} - h - W/2) \qquad \text{(Eq. 3)}$$

where D is the tendon duct external diameter, Pt is the tendon duct wall thickness, h is the distance between face of magnet and tendon duct outer surface, and W is the thickness of the magnet, all properties known for FTIU construction, direct tendon measurement, and for Pt tendon construction detail information or estimate. The value of d_C is then used to construct a diagram of the rebar bundle envelope when creating a diagram of the tendon cross-section.

The impedance information is transferred to the computer in the form of an array of recorded impedance modulus Z values in ohms, synchronous to the time array. Experiments conducted under [3] indicated that for tendons of size comparable to those in the Ringling Bridge the value of Z when the capacitor plate rides over a region of sound grout is in the order of Z_L = 15 kohm, while when the sensor is over a full void, extending from the strand bundle envelope to the inner surface of the duct, the impedance is in the order of Z_H = 30 kohm. Both values are user selectable for more refined void detection, as shown in Appendix 1. Additional tests under [3] indicated that a space filled with water tended to show a value <0.95•Z_L. Those values were used for default settings in the data processing program for the purposes of image display, implemented as a polar plot exemplified in Figure 7.

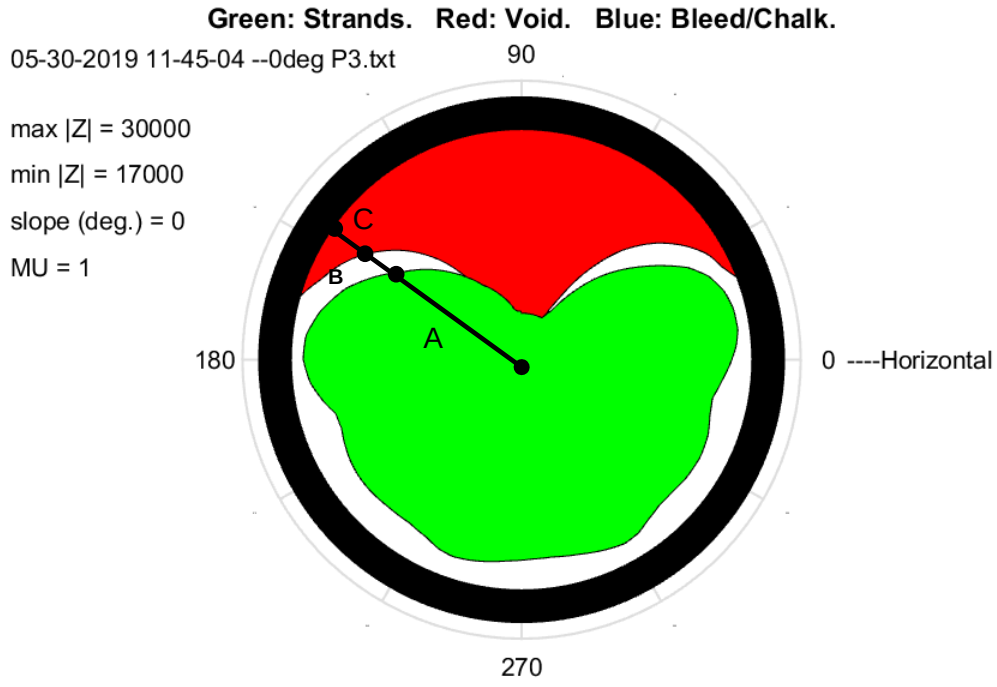

Figure 7 Example of cross-section image representation. Patent Pending.

The outer black ring is scaled to correspond to the actual dimensions of the polymer duct. At each rotation angle Θ_R the length from the center of the section to the inner duct diameter at each angle of the rotation pattern is divided into three regions. Region A, color-filled green, corresponds to the strand bundle, and the radial length of A (r_A) is obtained by Eq. 3. Region B (white) represents sound grout, while region C represents a void. The radial length of segment B plus C is equal to the inner duct radius, R_0 minus r_A. The partition between the lengths of B and C is allotted by

$$C/(B+C) = [(Z(\Theta_R)-Z_L) / (Z_H-Z_L)]^m \qquad \text{(Eq. 4)}$$

with the void zone always assigned by convention to the side closest to the duct. For purposes of image smoothing, before application of Eq. 4, the value of Z is set to Z_L if $0.95 < Z/Z_L < 1.15$. The fractional exponent m=0.75 was inserted to achieve greater graphic emphasis of the irregularity manifestation as the capacitive plate transitions between, for example, from being over a well-defined void to a sound grout region. Given the large angular span of the plate (~ 60-degrees) the transition boundary becomes blurred, in a manner comparable to that of a convolution of rectangular pulses [7]. Elevation to a fractional exponent creates a form of crude deconvolution for visual representation. A value of m=0.75 was chosen for the present implementation of the sensor. It is noted that this display choice is a semiquantitative adjustment subject to update in future development, and application to archived raw data.

To obtain a color coded overall pattern Eq.4 is used to obtain the radius values at the boundary of each region and color fill assigned per the provisions of the MATLAB platform. Nominal floor and ceiling levels of 1 cm and R_0 respectively were set for the strand bundle envelope radial dimensions in case calibration variability or measurement noise created visually unrealistic local patterns.

If the value of Z at a given rotation angle is $<0.95\ Z_L$, the region C is color coded blue designating a high water density region (either a water filled void or region with chalky grout), with partition assigned per Eq(4) but with Z_L and $0.8\ Z_L$ substituting for Z_H and Z_L respectively. For those situations the value of Z is set to $0.8 \bullet Z_L$ if $Z < 0.8 \bullet Z_L$ before application of Eq. 4. This display mode should be considered as an experimental feature as the differentiation between normal grout and high water content grout spans a small impedance range at the 1-MHz range used.

3.3 Performance

As discussed in further detail in material presented in Chapter 4 and in Project BDV25-977-24 [3], the FTIU provides consistent and reasonably descriptive images of the strand arrangement within the tendon. With appropriate calibration (via selection of representative values of Z_H and Z_L, with the help of tests conducted in the laboratory with mockup tendons) the FTIU also reliably detects full voids of dimensions comparable to the footprint of the capacitive plate and larger. Those voids are flagged with a sizable amount of red space on the zone between the strand bundle envelope and the inner surface of the duct. Detection of full voids narrower than the capacitive plate, or wide inner voids (voids present between the strand bundle and the duct but not reaching all the way to the inner surface of the duct) is limited, and in such cases the red space in the image is drawn to occupy only a fraction of the region between strand bundle and duct. The void detection process can be further refined if there are tendons in a bridge with previously known regions both with sound grout and with well-defined voids. In such case the user can image cross-sections of those regions, and experimentally reset the values of Z_H and Z_L for optimal thresholding of white and red

domain displays. The FTIU thus calibrated can then be used to more reliably image a group of peer tendons with unknown conditions. Building on this concept, a fine calibration procedure to automatically set the value of Z_L (and with Z_H set to $2 \bullet Z_L$ as a practical choice) has been implemented in the prototype for use on tendon locations where there is reasonable expectation of a sound grout condition. The procedure is described in Appendix 1.

Detection of high water content grout is mainly an experimental feature given that such content causes only a fractional reduction in the impedance at the frequency used in the FTIU. Future development with use of higher (and/or multiple) test frequencies is anticipated to result in significant improvement [3]. Meanwhile, this feature in its present form may still produce useful visual detection if there are tendons in a bridge with both regions of known high moisture grout as well as sound grout. The user can then image those regions and, analogous to the procedure described above for improved void detection, experimentally set the value of Z_L for optimal thresholding of blue zone display between the sound and high moisture zones.

The FTIU basic design accommodates tendons 4.5-inch in diameter, with duct wall thickness of 0.7 cm. Small variations in those values, or the presence of grout with magnetic properties, can be taken in consideration by changing the user choice parameter values as described in Appendix 1. Design is customizable to accommodate smaller tendon diameters down to 3.5-inch with minor modifications in roller and capacitive plate support. In those cases the parameter entries can be readily changed by the user.

It is noted too that this basic system arrangement is not limiting. It is amenable to expansion to the use of multiple magnets and capacitive plates, to allow for faster operation by reducing or obviating rotation need to produce a cross-section image.

Table 1 Data acquisition and processing parameters.

Parameter Symbol	Typical / default Value	Units	Notes
R_0	4.95	cm	Inner radius of tendon duct
D	12.7	cm	Outer tendon duct diameter
Pt	0.70	cm	Wall thickness of tendon duct
μ_{grout}	1.00	-	Relative magnetic permeability of grout
n'	3.185	-	Exponent of power law dependence between force and distance between magnet and strand envelope bundle
k	621.5	sensor units • $cm^{n'}$	Proportionality constant of power law dependence
τ	0.065	s	Force sensor time constant
W	0.32	cm	Magnet thickness
h	0.2	cm	Distance between magnet face and outer duct surface
Mw	69	sensor units	Magnet weight
MPU6050_Radius	2	cm	Distance from accelerometer sensor and outer duct wall
Θ offset	180	degrees	Angle offset difference between force and impedance sensors
Θ_S	Varied	degrees	Tendon inclination slope
Θ_R	Varied	degrees	Angle of FTIU rotation from starting position
m	0.75	-	Fractional exponent for graphic display
ag	9.797	m/s^2	Acceleration of gravity
Z_H	30	kohm	Impedance for full void location
Z_L	15	kohm	Impedance for sound grout location

4. FIELD ACTIVITIES AND PERFORMANCE

4.1 Activities

Activities under this project included three site visits as follows, with outcomes indicated in the following subsections:

1. Visit to Sunshine Skyway Bridge on 8/21/18.

2. Visit to John Ringling Causeway Bridge on 3/20/19

3. Visit to John Ringling Causeway Bridge on 4/30/19

4.2 August 21, 2018 site visit to Sunshine Skyway Bridge Pier 105/106

The purpose of the visit was to do a preliminary examination of tendons dimensions, clearances and surface conditions in the field for identifying which tendons are applicable for testing. In anticipation of subsequent activities, the opportunity of the visit was used also to make preliminary evaluations of the functionality of an initial version of the FTIU (with thin copper sheet capacitive plate) that was developed jointly with project BDV25-977-24 [3].

Areas visited were:

- South End of main group span 106.
- NB and SB high approach spans 105.

Most accessible tendons in the bridge were repair-wrapped with an ~0.125-inch thick polymeric sheet with folds that made the outside surface too irregular for normal FTIU operation. Moreover the wrap was made in ~3 ft sections, with an overlap of wraps ~2-inch to ~6-inch long causing furthered variations in the size of the tendons. A tendon was however evaluated that had a ~3.5-inch nominal diameter, but having a wrap with an irregular rough edge. It was nevertheless possible to clamshell the unit around the tendon and conduct some trial runs, despite the wrap edge and irregularities interfering with the development unit copper plate which became creased and bent limiting further tests. Notwithstanding those limitations, the IFU demonstrated battery-powered full functionality under field conditions, including providing a nominal cross-section image of the tendon inner components. This visit helped the corrosion team at USF to become familiar with field operating conditions and to identify the need for redesign of the capacitor plate within the unit to a more robust and firmer configuration more suitable for these conditions. Redesign and testing of a new plate and unit (described in Chapter 3) took place subsequently for use in the next field visits.

4.3 March 20, 2019 site visit to John Ringling Causeway Bridge

Tests:

The visit started with arriving to the south end island side of the Ringling Bridge (part of State Road 789, nominally E-W orientation road) at Bird Key Park. Entrance to Span 1 of the bridge is through a passage in the floor with the use of a 12 ft ladder. All equipment was brought up the ladder into Span 1. The equipment used included the Mark III Field Unit, the project laptop computer, all of the necessary connection wires, a set of work lights, and an 110v extension cord for the lights. Additionally, the Mark II Field Unit and extra hardware were brought as a spare if necessary (including a soldering iron).

Once inside of the bridge, two tendons were identified for testing, both located on the nominally N side in the center section of Span 1. Figure 8 shows the orientation of the tendons, reproduced and augmented from [8]. The first tendon tested (402L) was located near the floor, (~1 ft) and both tendons had plenty of room for rotating the unit. The second tendon (401L) was located at head level (~6 ft) from the floor.

Tendon 402L was evaluated at two places, labeled Test 1 and Test 4. Test 1 (Figure 9) was approximately 6 ft W of the lower deviation block that was near the E end of the span. The tendon was nearly horizontal, sloping about 0.5 degrees down to the E. The tendon section was slightly elliptical, measuring from 113 mm to 116 mm in diameter and not repair-wrapped. In here, as in the other places evaluated, after a quick wiping with a cloth, the surface of the tendon was smooth enough for impedance scanning. The computer was placed on a ~12-inch x 12-inch metal sheet lying on the floor.

Four groups of data (three images each, 12 in total, Figure 10) were collected at the Test 1 place. In all cases, the magnet starting point was centered on the 12 o'clock position on the tendon, and the FTIU was oriented with the side that connects to the USB port facing toward the W end of the bridge. The data files were labeled "032019H_402L_End_X" with X = 1 to 12 per the test execution order.

The first three groups at Test 1 used the regular 10' USB unit connection cable coiled with two rectangular ferrite blockers on the coiled section and a round ferrite blocker on the end of the USB that connects to the FTIU. The fourth group used the short USB cable with no ferrite blockers.

For grounding, the first group at Test 1 used an aluminum foil sheet on the floor (shiny side down) and a thin piece of metal on top to weigh it down to the floor to form a wired capacitive coupling ground with bridge. The second group was taken with a wired electrical ground (connected to the ground of the work lights, connected to the ground of the electrical system of the bridge). The third and fourth groups had no wire connection to the ground terminal in the unit, relying on the capacitive coupling provided by the computer via the USB cable.

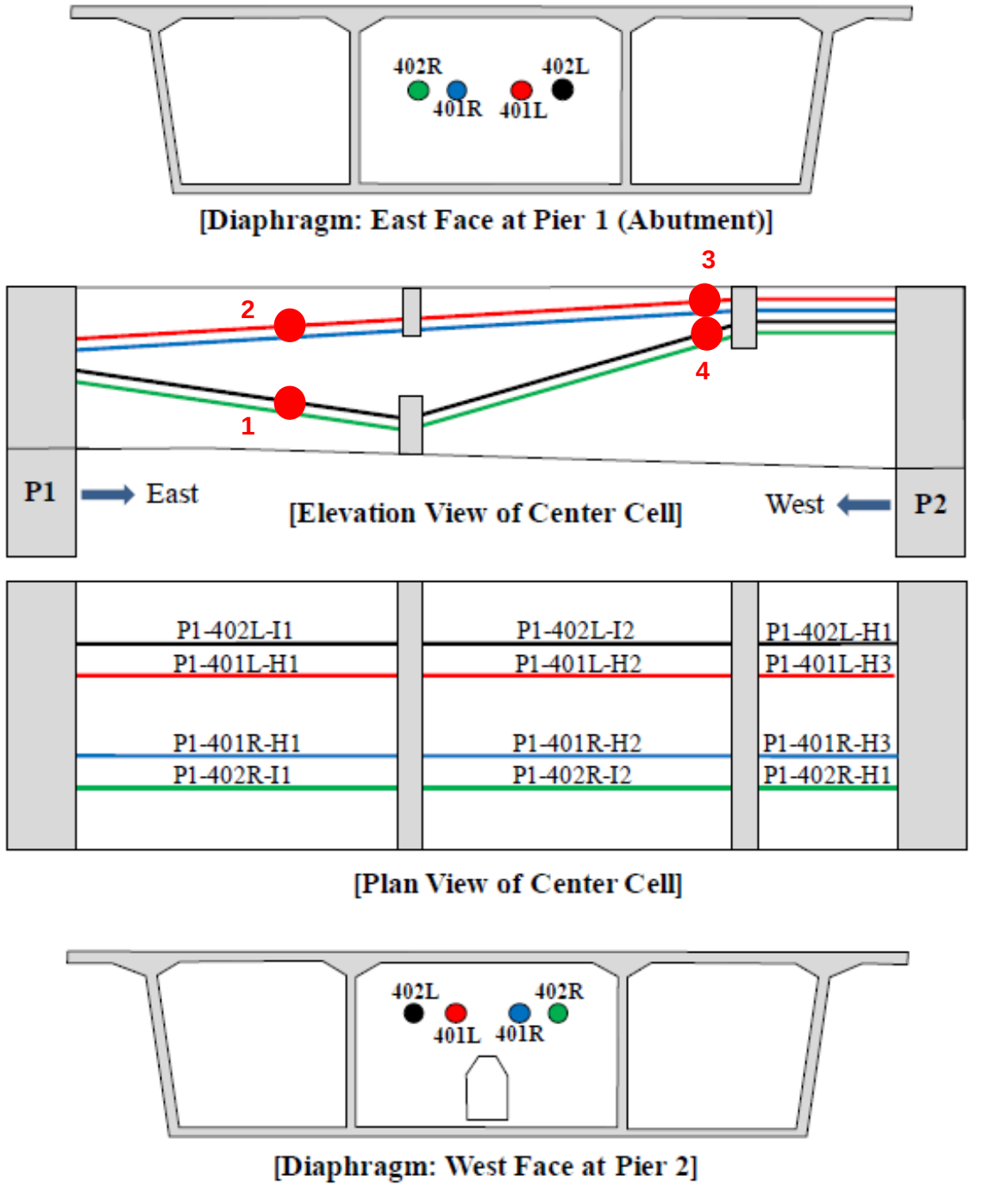

Figure 8 Tendon Layout in Span 1. Reproduced and augmented from [8]. Test places identified by red circles and Test numbers designating the 4 places evaluated.

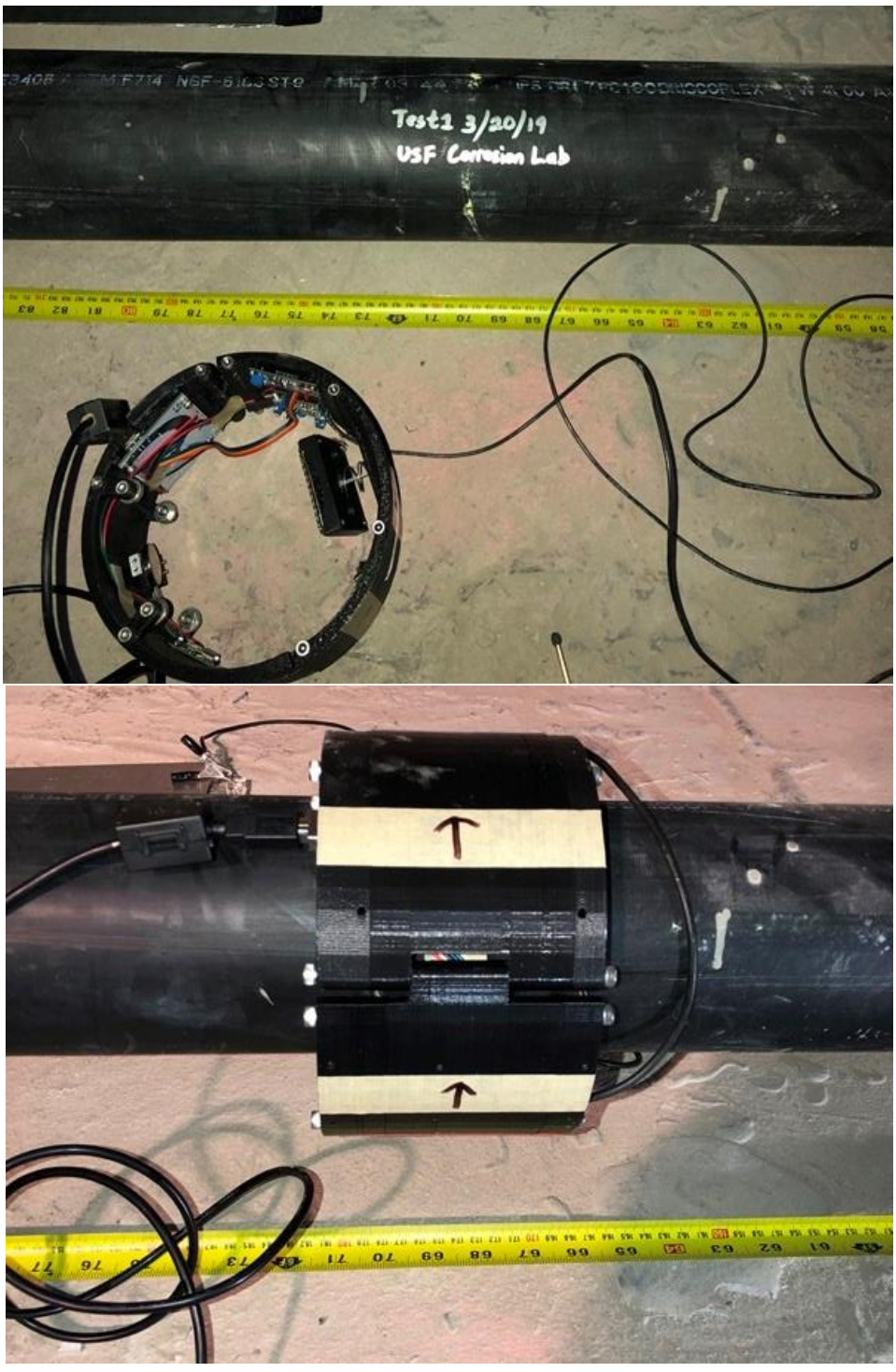

Figure 9 Test place at tendon 402L showing the field unit before (top) and after (bottom) clamshell-mounting. Patent Pending.

Tendon 401L was tested at two places. The first (labeled Test 2) was directly above the single place (Test 1) on tendon 402L. The Test 2 place was about 6 ft off the ground. The tendon measured 113 mm to 117 mm in diameter. The tendon sloped upward to the E about 2.5 degrees from horizontal. One group of images (file names 032019H_401L_End_X, X = 1 to 3) was collected with the magnet orientation the same as for 402L. This group used the same electrical ground as group 2 of 402L.

After evaluations at the Test 1 and Test 2 places in the center of Span 1, another two places were evaluated, Test 3 on Tendon 401L and Test 4 on tendon 402L, as shown in Figure 8. These two places, one on top of the other were located further E into Span 1, closer to Span 2 and about 2 ft W from the upper deviation block.

The Test 3 place on 401L was imaged with the operator standing on an 8 ft step ladder and the computer elevated 6 ft by an assistant. Tendon 401L measured 114 mm to 116.5 mm in diameter. One group of images (file names 032019H_401L_End_X, X = 4 to 6) was collected with the magnet oriented the same as in the other cases. This group used the same electrical ground as group 2 of 402L.

The Test 4 place on 402L was imaged with the operator and computer as in Test 3. The tendon measured 113.5 mm to 116 mm in diameter. The tendon sloped upward to the E about 9 degrees from the horizontal. One group of images (file names 032019H_402L_End_X, X = 13 to 15) was collected with the magnet oriented same as for 401L. This group used no wire ground (after the electrical ground wire became detached from the field unit during the first data set).

Results and Discussion

Figure 10 shows the 12 images generated at Test 1 place on tendon 402L. The results illustrated the stability of the response under grounding and wiring variations, as well as repeatability within each row. All images were successfully acquired with tendon rotations completed within a 10-second period. All images consistently identified the main pattern of strand locations (green) with a lopsided strand clustering to one side and top and a matching grout space opposite. The part of the clustering toward the top is consistent with the proximity and orientation of the bend of the nearby deviation block. No significant grout voids (which would have been colored red over a sizable portion of the image) were apparent, with the exception of vestigial indications as in Figure 11 that may be ascribed to marginal calibration and ground choices. It is noted that the duct was not breached to verify that interpretation.

Similar reproducibility of results was manifested at the other test places. Figure 11 shows in detail one of the images obtained for the same tendon 402L, but at the Test 4 place. Here, the strands tend to cluster toward the bottom of the cross-section, as would be expected, given the proximity to a block that deviates the strands opposite to the case in the Test 1 place. As in Test 1 place, there was no strong indication of a grout void.

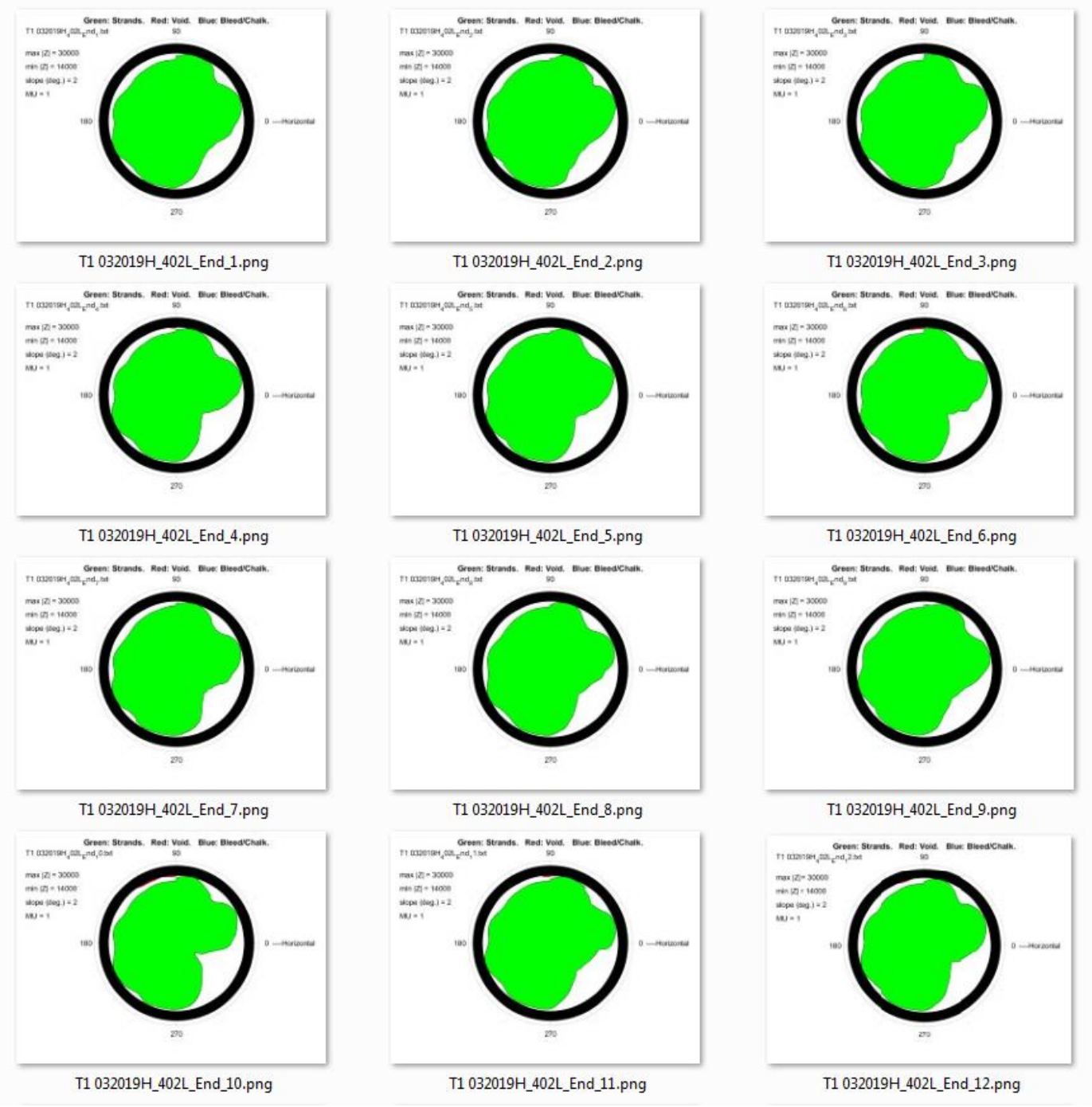

Figure 10 Images generated at Test 1 place on tendon 402L. Each row is for a group numbered as identified in the text, illustrating robustness of results to wiring and grounding variations, as well as illustrating repeatability within each condition. The strand bundle is colored green, while sound grout is white. No grout deficiencies were strongly apparent at this test place.

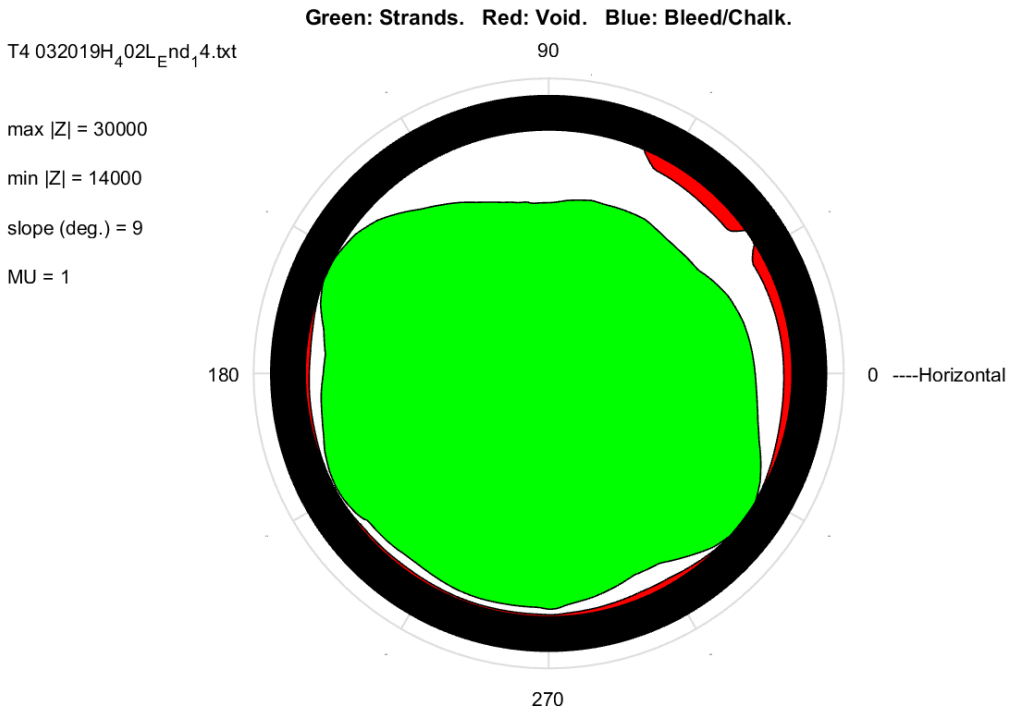

Figure 11 Image generated at the Test 4 place on tendon 402L. (032019H_402L_End_14). Minor red domain is not considered a strong indication of void presence.

Figures 12 and 13 show examples of the tendon cross-sections imaged for tendon 401L at the Test 2 and Test 3 places respectively. Reproducibility was comparable to that seen in the other cases. The strand pattern in the Test 2 place is less irregular than in the Test 1 place for 402L, possibly because it is less strongly deviated than 402L, as shown in the diagram in Figure 8 401L.

At the Test 3 place, the cross-section clusters to one side and to the bottom, consistent with what would be expected from the proximity and orientation of the nearby deviation block.

As in the tendon 402L cases, none of the places examined in 401L yielded any indication of significant void presence.

Since neither of the 2 tendons evaluated in the Ringling Bridge showed strong indications of grout deficiencies that permitted demonstrating the ability of the field unit to identify those defects, reference is made to the following excerpt of material from the Draft Final Report being prepared for project BDV25-977-24 [3]. Figure 14 exemplifies the results obtained with the field unit placed on a tendon mockup that incorporates sections of sound grout, a full air void, and a void filled with unhydrated grout. The figure illustrates the ability of the field unit to recover the strand pattern as well as the presence and extent of grout deficiencies. The cited document has further details.

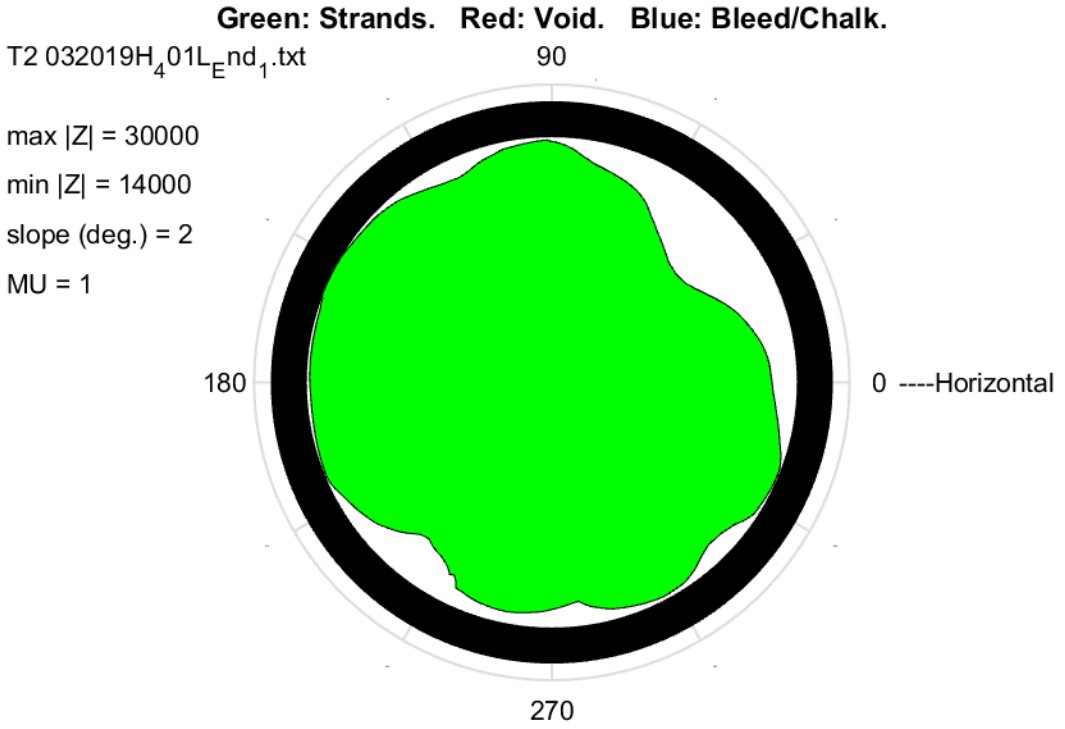

Figure 12 Image generated at the Test 2 place on tendon 401L. (032019H_401L_End_1)

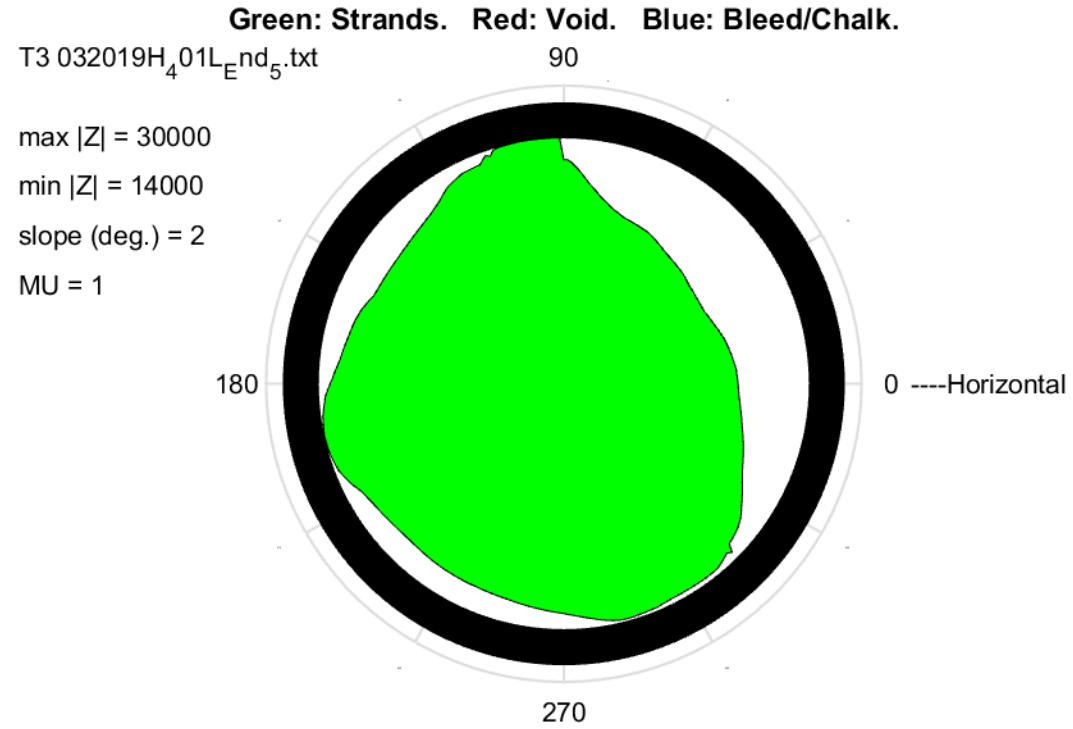

Figure 13 Image generated at the Test 3 place on tendon 401L. (032019H_401L_End_5)

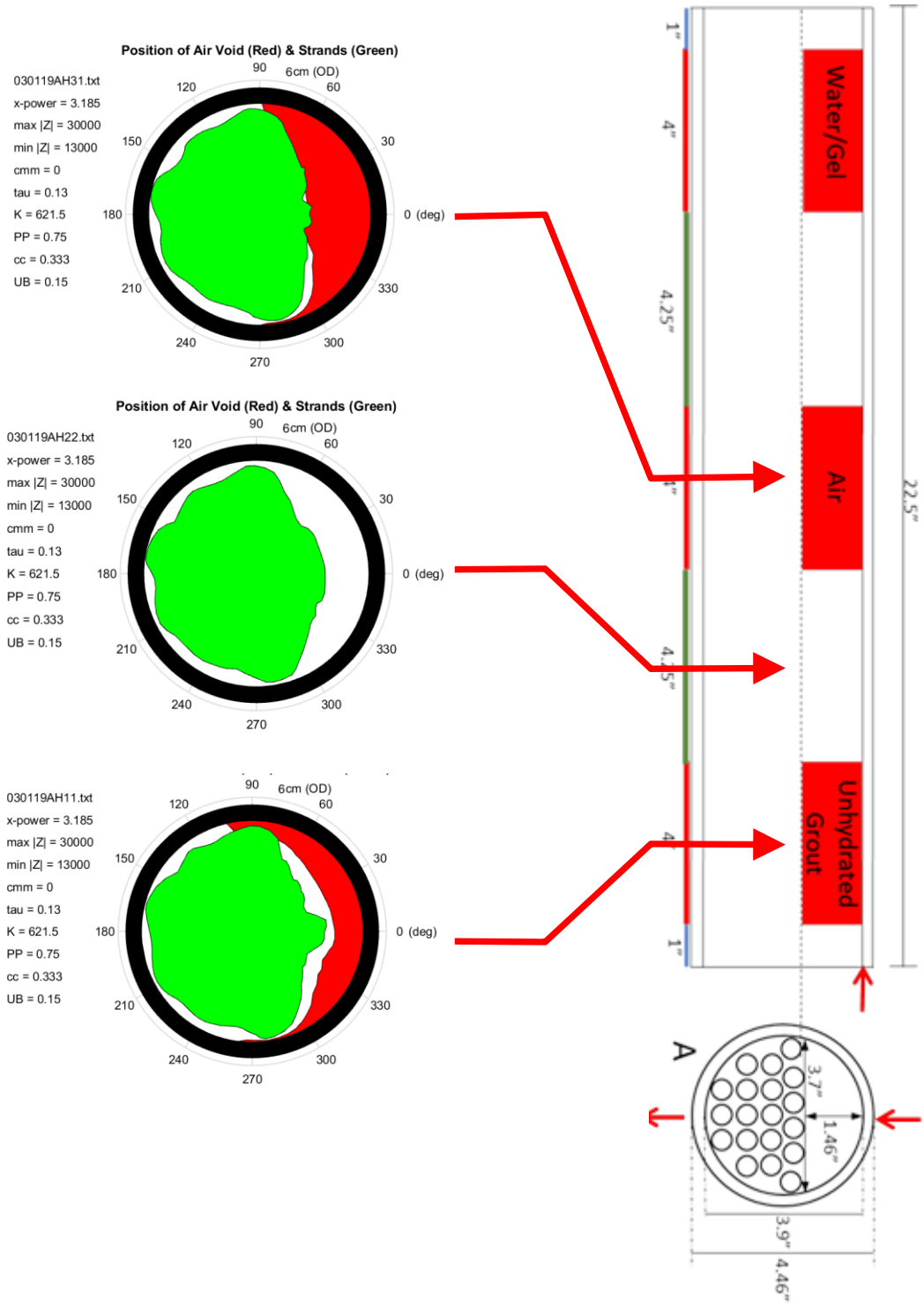

Figure 14 Material excerpted from the Draft Final Report being prepared for project BDV25-977-24 [3]. Images rotated to match orientation of the cross-section diagram.

4.4 April 30, 2019 site visit to John Ringling Causeway Bridge

Following further optimization of the FTIU this additional field visit was conducted for the Ringling Bridge, jointly with personnel of the FDOT State Material Office, to test operation experience by FDOT field personnel and identify closing list of items to be improved prior to delivery of the unit to FDOT. The test consisted of repeat imaging of various locations examined in the previous visit, with emphasis in evaluating user experience for improved performance. The following factors were noted and improvements in instrumentation and software were conducted accordingly with the following results:

- Simpler set up.
- Simple one-touch trigger for regular imaging function.
- No timeout rush for completing rotations.
- Automatic tendon slope angle measurement and recording for inclined tendons without need of manual determination.
- User enters first place number at the beginning of a series of image acquisitions on a tendon.
- Next places on tendon automatically numbered sequentially unless user flags test as a repeat.
- Normal numbering resumes automatically after that.
- User adds notes if desired before moving to next place on tendon.
- Straight up image orientation.
- Automatic force and rotation data correction for horizontal, inclined and vertical tendons.
- Tactile feel of sensor top.

All those features have been implemented as described in Chapter 2 and in the Operation Manual in Appendix 1.

5. CONCLUSIONS

1. An operating Field Tendon Imaging Unit (FTIU) was designed, constructed, and delivered to FDOT. The FTIU uses impedance and magnetic measurements to produce an image of the cross-section of an external post-tensioned tendon in a portable computer, flagging air voids and other deficiencies in the grout portion that is between the outer strand bundle envelope and the inner surface of the tendon polymer duct. The cross-section image includes the envelope of the strand bundle inside the tendon (from the magnetic measurements), and a color-coded indication of the condition of the grout in the space between the strand bundle and the inner surface of the tendon duct (from the impedance measurements).

2. The FTIU contains a magnet with force sensor and a flexible capacitive plate that follow the tendon duct perimeter during rotation around the tendon. The system accommodates external tendons with a 4.5-inch outer diameter. It has a flexible design to fit other common sizes in FDOT bridges. The FTIU is short and uses a clamshell arrangement to fit around the tendon with small (e.g., <1.5- inch) overburden, thus allowing for imaging in tight spaces without interfering with other tendons or structural members. Robust construction is suitable for extended field use. The concept is expandable to use of multiple magnetic and capacitive sensors for faster operation.

3. It takes only about 10-seconds to acquire a cross-section image, which is obtained by manually rotating the FTIU around the tendon and is displayed immediately by a laptop computer. The computer powers the FTIU by normal low-demand battery function, so the system is fully portable.

4. Operation does not require specialized operator training, and equipment can be reproduced at low cost and loaded with executable software produced by the project, thus providing an economic and rapid tendon assessment method capable of simultaneous deployment of multiple units.

5. The FTIU provided consistent and descriptive images of the strand bundle envelope within the tendon. With appropriate calibration, the FTIU also reliably imaged full voids of lateral dimensions comparable to those of the capacitive plate and flagged those by color-coding the zone between the strand bundle envelope and the inner surface of the duct. Sensitivity to smaller or internal voids are limited; when detected, a partial color display scheme is shown. Refined detection can be made if calibration is possible with a field tendon with known deficiency regions.

6. Detection of high water-content grout is mainly an experimental feature, given that such content causes only a fractional reduction in the impedance at the frequency used in the FTIU.
7. An initial field visits, was made to the Sunshine Skyway Bridge to familiarize USF personnel with field operating conditions and identify the need for robust design features.
8. Two subsequent field visits were made to the Ringling Bridge, demonstrating application on four test places with multiple variations of system wiring and grounding, as well as establishing repeatability.
9. The field results demonstrated stability of response under grounding and wiring variations, as well as repeatability within a given condition. All images were successfully and rapidly acquired, consistently identifying the main pattern of strand locations for a given test place. The FTIU retained physical integrity through extensive repeat field testing and no breakdown or need for repair took place.
10. Tests conducted on the tendons at different places with respect to deviation blocks revealed strand clustering consistent with the orientation of the deviation block, and with the extent of the deviation.
11. All the field images obtained at the Ringling Bridge were consistent with sound grout, with no void or similarly detectable deficiency at any of the places examined, likely reflecting prior extensive repairs there. Consequently illustrations of ability to identify selected types of deficiencies on a laboratory tendon mockup were presented instead.

REFERENCES

[1] A. Sagüés "Posttensioned Grouted Tendons", in *ASM Handbook, Volume 13C, Corrosion: Environments and Industries,* pp. 570-571, Materials Park, OH: ASM, The Materials Information Society, 2006.

[2] K. Krishna Vigneshwaran, S. Permeh, M. Echeverría, K. Lau, I. Lasa, Corrosion of Post-Tensioned Tendons with Deficient Grout, Part 1: Electrochemical Behavior of Steel in Alkaline Sulfate Solutions, Corrosion, Vol 74 (3), pp. 362-371, 2018.

[3] H. Freij, D. Dukeman, A. Sagüés, “Development of Tendon Imaging Sensor” Draft Final Report, FDOT Project BDV25-977-24, submitted July 2019.

[4] A. Sagüés, *Systems and methods for determining strand position in a post-tensioned tendon* Patent No.: US 9,651,357 B1, 2016.

[5] H. Freij, Ph.D. Dissertation, *Detection of Grout Anomalies Using Non-Destructive Testing in External Post-Tensioned Tendons in Bridges,* University of South Florida, Tampa, 2019.

[6] F. Presuel-Moreno, A. Sagüés, Bulk Magnetic Susceptibility Measurements for Determination of Fly Ash Presence in Concrete, Cement and Concrete Research, Vol. 39 (2), pp. 95-101, 2009.

[7] C. McGillem and G. Cooper, *Continuous and discrete signal and system analysis*. Holt, Rinehart and Winston, 1974.

[8] K. Lau and A. Azizinamini. Development of Quality Assurance and Quality Control System for Post-Tensioned Segmental Bridges in Florida: Case of Ringling Bridge – Phase II (Florida Department of Transportation Research Report BDV29-977-34). Florida International University, Miami, Florida, 2018.

APPENDIX 1

FIELD TENDON IMAGING UNIT OPERATING MANUAL

An operating FTIU with computer, cabling and installed executable code have been provided to FDOT as a deliverable under the present contract. Instructions for use are presented in the attached Operating Manual.

Project

Field Demonstration of Tendon Imaging Methods
FDOT Contract Number: BDV25-977-52
USF Contract Number: 2104 1287 00

FDOT Project Manager: Adrian Steele, SMO, Gainesville, FL.
Continuing PI: Christopher Alexander, University of South Florida, Tampa, FL.
Initiating PI: Alberto Sagüés (Retired).

FIELD TENDON IMAGING UNIT OPERATING MANUAL

VERSION v053119

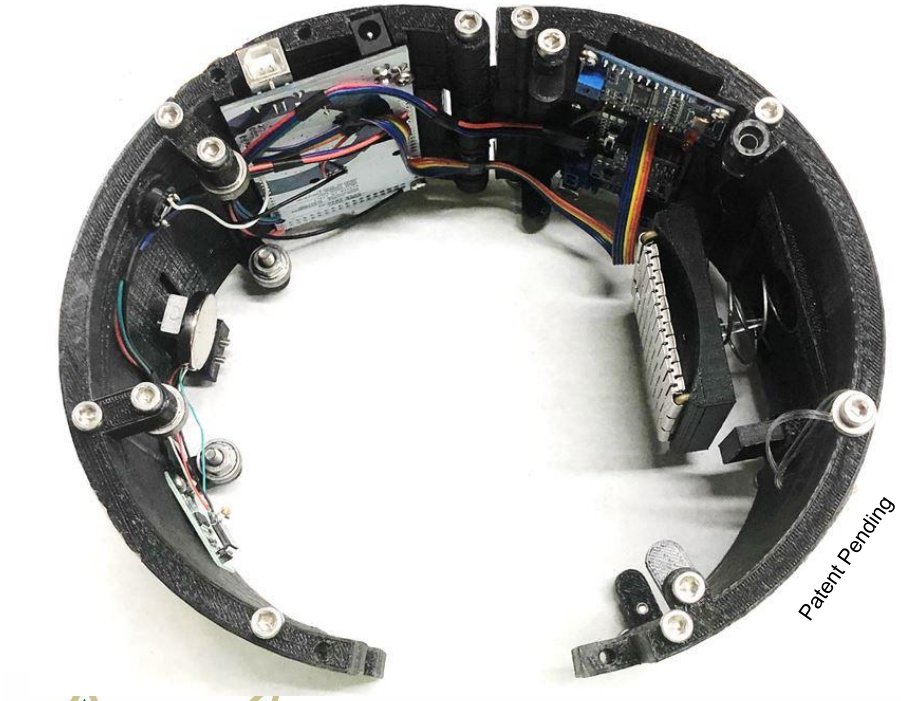

UNIVERSITY OF SOUTH FLORIDA

College of Engineering
University of South Florida
Tampa, FL
July 2019

Prepared by:
D. Dukeman
H. Freij
A. Sagüés
C. Alexander

SYSTEM PARTS

The following items are provided:

- MARK III Field Unit. Laptop computer
    - It contains:
        - Shortcut “Tendon Imager” to executable saved on the desktop.
        - MATLAB executable file “TendonImager_v053119.exe” saved on the desktop in the folder “*Field Operations*”.
            - Arduino v1.8.5. saved on the *“C:”* drive.
            - MATLAB MyAppInstaller_mcr.exe, copy saved in the *“Documents*” folder.
            - Arduino sketch “*FieldUnitPro7c.ino*” already uploaded to the Field Tendon Imaging Unit (FTIU) and a copy saved in the *“Documents*” folder.
- Cable “USB Type-C male to USB Type-B male”.
- Ground wire with banana terminal on one end and alligator on other end.

SOFTWARE INSTALLATION

Software is already installed in the FDOT computer delivered with this project. This item is included in case of need of transfer to another computer.

Files needed:

- MyAppInstaller_mcr.exe
- TendonImager_v053119.exe

Step-by-Step installation:

1. Create a folder named “Field Operations” on the computer Desktop.
2. Copy both provided files into that folder. Double click “MyInstaller…” and wait until completion, answering installation prompts as required.

SYSTEM OPERATION
A - Hookup and Placement

1. Plug FTIU into the laptop USB-C port. Inside LEDs will turn on, confirming power connection.
2. On Desktop screen, double click on shortcut ***"Tendon Imager".*** Wait for query window on screen (~13 seconds).
3. Query window **(Figure 1)** asks for starting place number on tendon to be imaged.

   Assign number 1 (default value) to first tendon place to be tested in the day. As long as you stay in the same tendon, program will automatically assign consecutive numbers to all the following places. If you are resuming testing at a different location and you want for that series to start with a new number (say number 57), enter 57. After desired number is entered **Click OK.**

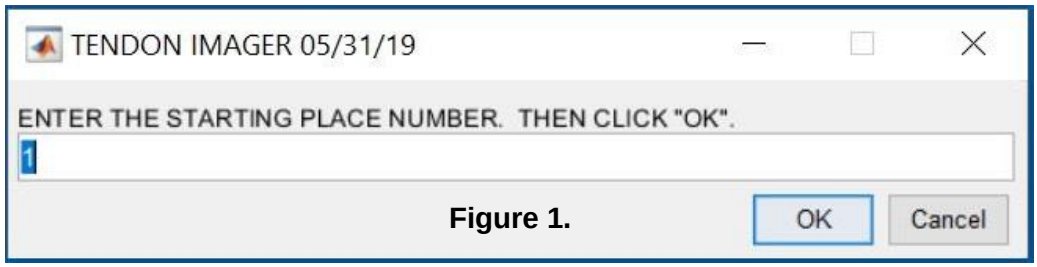

Figure 1.

4. Next query window **(Figure 2)** asks operator to use stored global tendon properties.
   - To use most recently stored values **click YES or Press Space Bar.**
   - To view or change values **click VIEW / CHANGE** (see section C for details).
   - To use "factory" default values **click USE DEFAULT** (see section C for details).

Figure 2.

5. Next query window **(Figure 3)** asks for tendon orientation.
    - For horizontal or sloped tendons **click HORIZONTAL/SLOPED or Press Space Bar** and FTIU will determine slope of tendon automatically.
    - For vertical tendons **click VERTICAL** and keep blue line on FTIU always starting facing the same direction. This line is start position for vertical tendon images.

Figure 3.

6. Next query window **(Figure 4)** asks operator to place FTIU vertically on floor or horizontal surface with USB connector facing up, then **click OK or Press Space Bar.** Wait until the next step is ready.

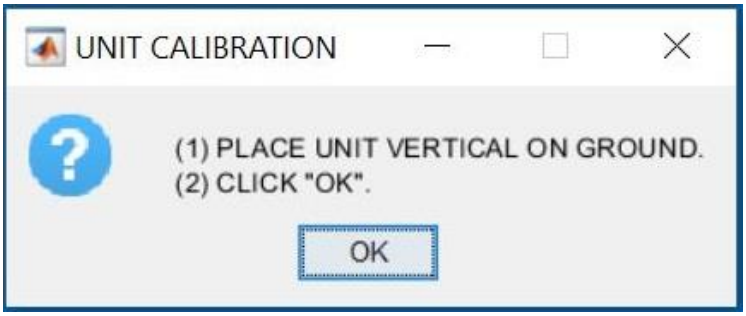

Figure 4.

7. Next query window **(Figure 5)** asks user to position the FTIU on tendon starting place and get ready for acquisition of a series of tendon images. Before clicking OK, set up as shown in **Figure 6.**

Figure 5.

To get ready for an imaging series:

- **a.** Clean tendon surface to remove dust and debris.
- **b.** Remove brass locking pin of FTIU, open clamshell, wrap on selected tendon place No. 1 (or number designated). Close using pin.
- **c.** Horizontal/Sloping tendons: Orient FTIU per Figure. Blue line should be on top of tendon, precision positioning not needed.
- **d.** Vertical tendons: Keep blue line always starting facing the same direction.
- **e.** Attach ground wire to bridge ground or ground plate.
- **f.** Ensure USB and ground cable are loose enough to allow for one full turn.
- **g.** **Click OK or Press Space Bar.** The next query window will appear; proceed to **Acquiring Images**.

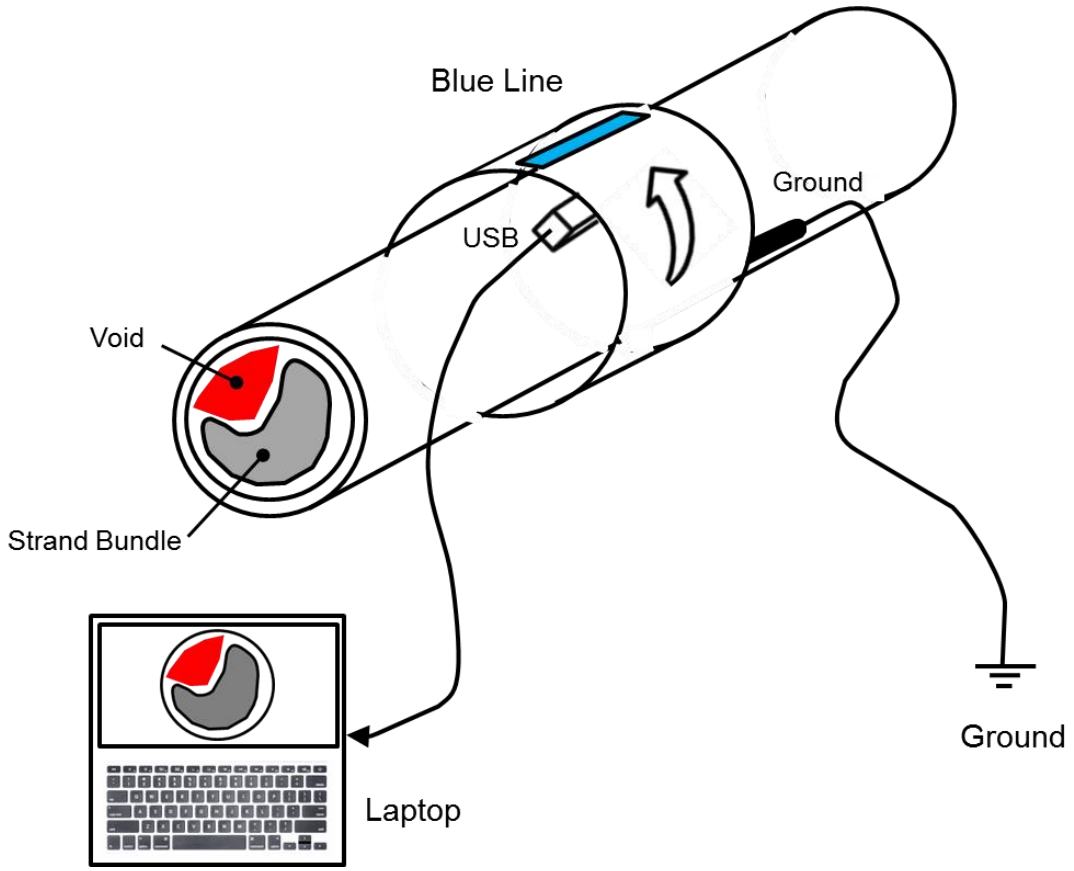

Figure 6.

B - Acquiring Images

Operations here can be conducted by single clicks/taps throughout.

8. After Hookup and Placement are complete the query window in **Figure 7** appears:

Figure 7.

Click OK or Press Space Bar. A Beep will sound. After beep, start rotating FTIU in the arrow direction. It will beep again when it senses a full turn. Stop and wind-back to start. Cross-section image will show on screen right away **(Figure 9).**

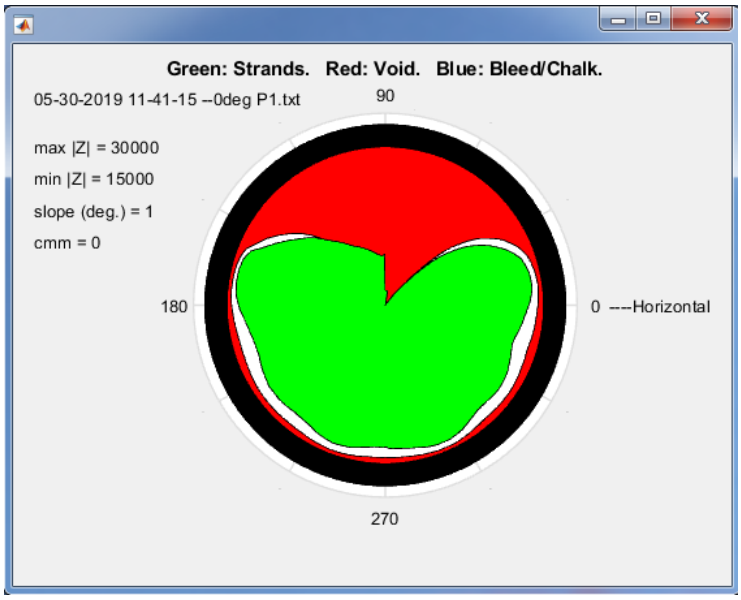

Figure 9.

Notes:

- Rotate FTIU in arrow direction.
- While rotating, press on blue marker to ensure firm roller contact over entire turn.
- No need to rush turning after Beep; FTIU will not timeout.
- Take about 10 seconds to do one turn, but speed is not critical and slower motion is ok. Do avoid extremely rapid turns. Wind-back speed is unimportant.
- Angular positions at the start or after wind-back are not critical. FTIU sensors find exact apex (vertical tendons excepted) and know when full turn was completed.

9. A new query window will appear next **(Figure 10).**

Figure 10.

- If image is acceptable **click IMAGE NEXT PLACE or Press Space Bar.** Slide FTIU to next place. Go back to Step 8.
- If a repeat is desired **click REPEAT LAST IMAGE**. Stay in the same place. Go back to Step 8. Repeat image will have "R1" added to file name. Multiple repeats are allowable and will be tagged R2, R3 etc.
- To add a comment, **click MAKE A NOTE.** That will launch a query window that accepts text and appends text to end of data file for the image just generated. This text will not affect image. Multiple notes can be appended to same data file if needed. After making the note the Figure 10 box appears again.

Notes:

- After each image is acquired the image is automatically stored, together with a data file used to generate the image, in the *"Field Operations"* folder on the desktop. Names of image and data files contain image place and time acquired.
- User needs to take note as to which tendon and tendon place was imaged for the first image, and where in the tendon with respect to the first image the other images were acquired.

10. The final window **(Figure 11)** appears when user is done and closes window in step 9. Final window acknowledges that program is ending and will close any remaining open windows or figures. **Click OK or close this window.**

Figure 11.

C – Adjusting Global Tendon Properties

1. To adjust global tendon properties locate the second query window seen in **Figure 12.** To view or change the current values **click VIEW / CHANGE**.

Figure 12.

2. Query window **(Figure 13)** asks for particulars of tendon to be imaged, showing the values stored from last time use. If all are as desired without changes, **click OK**.

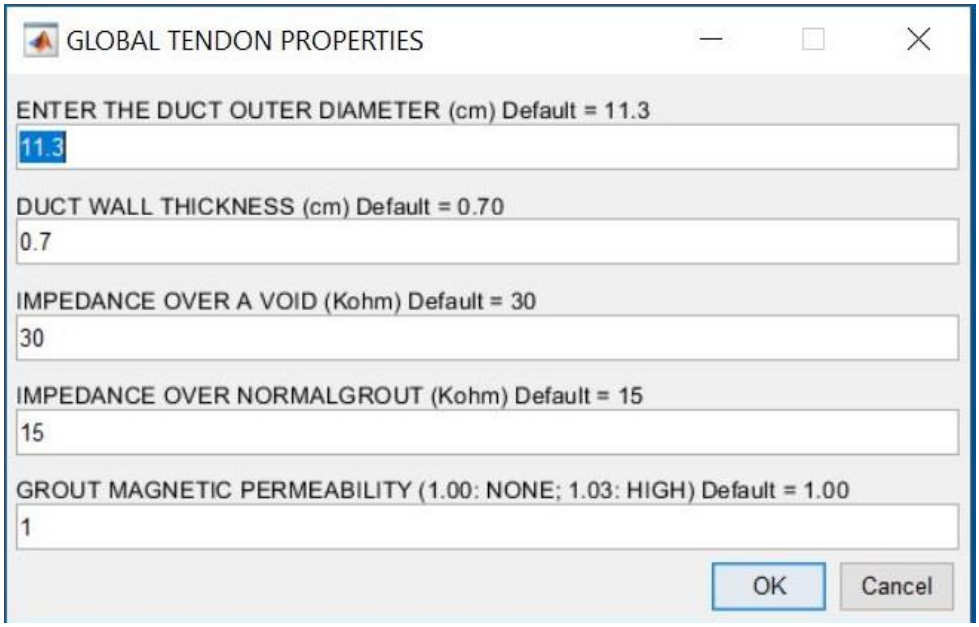

Figure 13 (example - numbers stored from last time use may be different).

- If editing is needed, enter appropriate values per notes in next page. New entries will become the stored values for this and subsequent uses. **Click OK** when done changing.

Notes on editing global tendon properties:

- DUCT OUTER DIAMETER: This entry defaults to 11.3 cm (4.5-inches, as in the Ringling Bridge). If tendon size is different ant still falls within the FTIU specs (say for example 10.9 cm), enter here that value.
- DUCT WALL THICKNESS: This entry defaults to 0.7 cm (0.275-inch, as in the Ringling Bridge). Enter alternative value if it is known.
- IMPEDANCE OVER A VOID: This entry defaults to 30 kohm, typical of value expected when the capacitive plate is over a full void per laboratory experiments results. Enter alternative value if recommended by a specialist.
- IMPEDANCE OVER NORMAL GROUT: This entry defaults to 15 kohm, typical of value expected when the capacitive plate is over sound grout per laboratory experiments results. Enter alternative value if recommended by a specialist.
- GROUT MAGNETIC PERMEABILITY: This entry defaults to 1.00, typical of behavior for most commonly used grouts, per laboratory experiments results. Enter alternative value if grout in tendons is known to exhibit magnetic behavior. If grout is known to be EUCO Cable Grout, enter 1.015 (mid-range of choices). Otherwise consult specialist.

- If the default values are desired instead (those happen to be the numeric values listed in Figure 13), **clicking USE DEFAULT** prompts a query window **(Figure 14)** asking to confirm that user wants the default properties. To accept default properties **click YES**.

Figure 14.